

1 **Drought-induced biomass burning as a source of black carbon to the Central**
2 **Himalaya since 1781 CE as reconstructed from the Dasuopu Ice Core.**

3

4 Joel D. Barker^{1,2}, Susan Kaspari³, Paolo Gabrielli^{1,2}, Anna Wegner², Emilie Beaudon²,
5 M. Roxana Sierra-Hernández², Lonnie Thompson^{1,2}

6

7 ¹ Byrd Polar and Climate Research Center, The Ohio State University, Columbus,
8 43210, USA.

9 ² School of Earth Sciences, The Ohio State University, Columbus, 43210, USA

10 ³ Department of Geological Sciences, Central Washington University, Ellensburg, USA,
11 98926

12

13 *Correspondence to: Joel D. Barker (barke269@umn.edu)*

14

15 **Abstract**

16 Himalayan glaciers are melting due to atmospheric warming with the potential to limit
17 access to water for more than 25% of the global population that reside in these glacier
18 meltwater catchments. Black carbon has been implicated as a factor that is contributing
19 to Himalayan glacier melt, but its sources and mechanisms of delivery to the Himalayas
20 remain controversial. Here, we provide a 211-year ice core record spanning 1781 –
21 1992 CE for refractory black carbon (rBC) deposition from the Dasuopu glacier ice core,
22 that has to date provided the highest elevation ice core record (7200 m). We report an
23 average rBC concentration of 1.5 µg/L (SD = 5.0, n = 1628) over the 211-year period.
24 An increase in the frequency and magnitude of rBC deposition occurs after 1877 CE,
25 accompanied by decreased snow accumulation associated with a shift in the North
26 Atlantic Oscillation Index to a positive phase. Typically, rBC is deposited onto Dasuopu
27 glacier during the non-monsoon season, and short-lived increases in rBC concentration
28 are associated with periods of drought within neighboring regions in north-west India,
29 Afghanistan and Pakistan. Using a combination of spectral and back trajectory
30 analyses, and comparison with a concurrent analysis of trace metals at equivalent
31 depths in the same ice core, we show that biomass burning resulting from dry

32 conditions is a source of rBC to the central Himalaya, and is responsible for deposition
33 that is up to 60 times higher than the average rBC concentration over the time period
34 analyzed. We suggest that biomass burning is a significant source of rBC to the central
35 Himalaya, and that the rBC record can be used to identify periods of drought in nearby
36 regions that are up-wind of Dasuopu glacier.

37

38 **1 Introduction**

39 Although the rate and extent of glacier melt differs geographically, the overall trend of
40 glacier mass loss globally, and particularly in mountain glaciers, is well documented
41 (IPCC, 2013). While warming summer temperatures resulting in increased glacier mass
42 loss (e.g. Gregory and Oerlemans, 1998) and decreasing precipitation as snow (Raper
43 and Braithwaite, 2006) are important factors contributing to glacier mass wastage
44 globally, the deposition of atmospheric aerosols that darken the glacier surface also
45 contribute to melt (Flanner et al., 2007; Xu et al., 2009; Xu et al., 2012), particularly in
46 proximity to aerosol emission sources. The most efficient of these aerosols is black
47 carbon (BC) which is produced by a variety of combustion processes (Bond et al., 2004,
48 2013), most commonly by the incomplete combustion of fossil fuels and biomass
49 (Jacobson, 2004; Hammes et al., 2007). BC is also the dominant absorber of visible
50 light in the atmosphere (Lindberg et al., 1999) and exerts a positive radiative forcing
51 globally, second only to CO₂ (+1.1 W m⁻² and +1.6 W m⁻² respectively; Ramanathan and
52 Carmichael, 2008). BC continues to absorb radiation upon deposition from the
53 atmosphere onto glacier surfaces, reducing ice and snow albedo, leading to melt
54 (Hansen and Nazarenko, 2004; Forster and Ramaswamy, 2007; Xu et al., 2009;
55 Doherty et al., 2013).

56

57 A significant source of BC emitted to the atmosphere results from anthropogenic activity
58 (Ramanathan and Carmichael, 2008; Bond et al., 2013). The BC flux to the atmosphere
59 has increased by a factor of 2.5 since the Industrial Revolution, resulting in an increase
60 of the global atmospheric BC burden by a factor of 2.5 - 3 (Lee et al., 2013). BC's
61 relatively short atmospheric residence time influences its distribution globally, with the
62 highest concentrations being proximal to BC emission sources (Bond et al., 2007; Xu et

63 al., 2009; Bond et al., 2013). Asian regions surrounding the Himalaya are major sources
64 of atmospheric BC (Novakov et al., 2003; Bond et al., 2007; Ramanathan et al., 2007;
65 Bond et al., 2013) and southern Himalayan glaciers are particularly influenced by BC
66 emissions from India (Kopacz et al., 2011; Gertler et al., 2016) and more local emission
67 sources that may add to the broader-scale regional flux (Kaspari et al., 2011).

68
69 Atmospheric aerosols, including BC, are warming the cryosphere and accelerating snow
70 melt in the western Tibetan Plateau and Himalayas (Lau et al., 2010) and altering the
71 regional hydrologic cycle (Immerzeel et al., 2010). This is a concern because Hindu
72 Kush Himalayan (HKH) glacier melt affects the water security, particularly during the
73 early- and post-monsoon season (Hill et al., 2020), of densely populated regions of
74 south-east Asia. Meltwater from HKH glaciers are the source of ten major rivers that
75 provide water for irrigation, hydropower, and ecosystem services for two billion people
76 across Asia (Scott et al., 2019); over 25% of the global population.

77
78 Research into BC's interaction with the HKH cryosphere has increased in recent years.
79 Several studies have documented the magnitude and timing of BC deposition using
80 short-term BC records preserved in surface snow that span 1 - 2 years (e.g. Xu et al.,
81 2009; Ming et al., 2008; Ming et al., 2012; Kaspari et al., 2014; Zhang et al., 2018; Thind
82 et al., 2019). More recently, continuous surface measurements of near-surface
83 aerosols, including BC, have been reported for the HKH region (e.g. Marinoni et al.,
84 2010; Bonasoni et al., 2010; Cao et al., 2010; Babu et al., 2011; Chaubey et al., 2011;
85 Marinoni et al., 2013; Niu et al., 2017; Negi et al., 2019). While useful for tracking the
86 evolution of atmospheric BC at high temporal resolution, these studies do not provide a
87 longer-term historical context against which current levels of BC can be compared.
88 Records of BC deposition preserved in ice cores are useful as longer-term
89 environmental archives for reconstructing atmospheric aerosol composition that span
90 decades (Liu et al., 2008; Ming et al., 2008; Ginot et al., 2014). In the HKH region, these
91 archives are essential for identifying trends in BC deposition onto HKH glaciers in
92 response to increasing BC emissions in surrounding regions. For example, Ming et al.
93 (2008) report an increasing trend in BC deposition onto East Rongbuk Glacier (Mt.

94 Everest; 6500 m above sea level (asl)) during a 10 year period beginning in 1965, and
95 then another increase beginning in 1995 to the end of the record in 2001. Xu et al.
96 (2009) report a period of relatively high concentrations in the 1950s and 1960s in 4
97 Himalayan and Tibetan Plateau glaciers (Muztagh Ata, Guoqu glacier, Noijin Kangsang
98 glacier, East Rongbuk glacier, and Tanggula glacier) and suggest a European source of
99 BC to these sites. They also note an increase in BC on the eastern-most site (Zuoqiupu
100 glacier) beginning in the 1990s and suggest an Indian source of BC for the region.
101 Similarly, Liu et al. (2008) report high elemental carbon at Muztagh Ata from 1955 -
102 1965. Ginot et al. (2014) report BC concentrations at Mera Glacier from 1999 - 2010,
103 and suggest that variations in BC over this period respond primarily to monsoonal rather
104 than anthropogenic forcing.

105

106 Kaspari et al. (2011) were the first to present a BC record that extended back to the pre-
107 industrial period (1860-2000) in an ice core from East Rongbuk glacier (6518 m asl) and
108 reported a threefold increase in BC deposition since 1975, indicating that anthropogenic
109 BC is contributing to the BC flux to the southern Himalaya. Jenkins et al. (2016) report
110 an increase in BC deposition in the central Tibetan Plateau beginning in 1975 from the
111 Guoqu glacier ice core record spanning 1843-1982. These deep ice core records are
112 valuable for evaluating long-term trends in BC spanning the Industrial Revolution to the
113 present and the concomitant increase in anthropogenically-sourced BC emissions.
114 Additional ice core-derived BC records that span the period of industrialization in Asia
115 are required to both corroborate existing historical records of BC deposition onto HKH
116 glaciers and to establish a regional baseline record for BC fluxes onto the region. These
117 records are currently lacking for the HKH and are essential for identifying regional-scale
118 trends in BC deposition.

119

120 The highest elevation ice core record ever obtained is the Dasuopu ice core (C3;
121 Thompson et al., 2000), which was retrieved from the Dasuopu Glacier in the Central
122 Himalaya (28.38 °N, 85.72 °E; Fig. 1) in 1997 at an elevation of 7200 m asl. Thompson
123 et al. (2000) determined that monsoonal precipitation is responsible for the net
124 accumulation of snow onto the glacier surface, in the order of 1000 mm water

125 equivalent per year (in 1996), permitting an annually resolved environmental record
126 spanning 1440 - 1997 CE (Thompson et al., 2000). The remote location and high
127 elevation of the Dasuopu ice core drill site suggests that any local influence on the
128 deposition of atmospheric aerosols onto the glacier surface is minimal, and that
129 accumulation is representative of mixed free tropospheric composition (Kumar et al.,
130 2015). Evidence suggesting that the Dasuopu glacier differs from lower-elevation
131 glaciers in the region with respect to seasonal meteorology supports the hypothesis that
132 the flux of aerosols onto the glacier surface may be more representative of free
133 tropospheric composition rather than being affected by local (valley-scale)
134 meteorological conditions (Li et al, 2011). Generally, the lower limit of the free
135 troposphere in the central Himalaya occurs at ~2.5 km in the winter and 3.3 km in the
136 summer seasons (Solanki and Singh, 2014).

137

138 Here, we quantify refractory BC (rBC; a subset of the broader BC descriptor of
139 carbonaceous particles that it is measured by laser induced incandescence specifically;
140 Petzold et al. (2013), Lack et al., 2014) in a section of the Dasuopu ice core from 1781-
141 1992 CE at annual to seasonal resolution in the glacier ice portion. We employ spectral
142 analysis of the rBC ice core time series to identify trends in rBC deposited onto
143 Dasuopu glacier across several temporal scales and to avoid “peak-picking” that might
144 lead to subjectively identifying episodes of increased rBC in the ice core time series.
145 The rBC record is compared to trace-element analysis of samples from equivalent
146 depths along the same ice core, as described by Gabrielli et al. (2020), and an
147 atmospheric back trajectory analysis to elucidate the broader-scale trends of deposition
148 and potential rBC sources to the southern Himalaya.

149

150 **2 Methods**

151 **2.1 The Dasuopu Ice Core**

152 Dasuopu glacier descends to the north from Mt. Xixiabangma in the Central Himalaya
153 (Fig. 1). The ice core examined here was drilled from the Dasuopu glacier surface to
154 bedrock (145.4 m) with an electromechanical drill, without using drilling fluid, and
155 provides a continuous record of deposition onto the glacier surface from 1010 to 1997

156 CE (Thompson et al. 2000). Here, we examine the upper section of the C3 ice core
157 (hereafter referred to as the “Dasuopu core”), from 8.4 - 120.3 m depth from the
158 surface, corresponding to the period 1781 - 1992 CE. Sections of the Dasuopu core
159 outside of this interval were not available for analysis. We use the Thompson et al.
160 (2000) chronology that was established using $\delta^{18}\text{O}$, dust, and NO_3^- measurements, as
161 well as annual layer counting confirmation using the location of the 1963 CE beta
162 radioactivity peak from thermonuclear tests at a depth of 42.2 m to determine the core’s
163 age-depth relationship. Thompson et al. (2000) also used two major monsoon failures
164 (1790-1796 and 1876-1877) as age/depth benchmarks that are reflected in the dust and
165 Cl^- records to validate the ice core dating chronology. The chronology is accurate to ± 3
166 years (Thompson et al., 2000).

167

168 **2.2 Sample Preparation**

169 A portion of the Dasuopu core has been housed in the Ice Core Storage Facility (Byrd
170 Polar and Climate Research Center (BPCRC)) at $-30\text{ }^\circ\text{C}$ since the original analysis by
171 Thompson et al. (2000). The portion of the Dasuopu core analyzed here is
172 characterized by consolidated firn from 8.4 m - 56.4 m and glacier ice from 56.4 - 120.3
173 m depth. Ice was sampled continuously (with the exception of intervals noted in Suppl.
174 Info. Table 1) in a cold room ($-5\text{ }^\circ\text{C}$) at sub-annual resolution (2.5 - 10 cm sample
175 interval) with a band saw along the length of the ice section. Each ice sample was
176 divided in half to permit the analysis of BC and trace elements from identical depths
177 throughout the core ($n = 1572$). Prior to rBC analysis, each ice sample was rinsed with
178 type 1 Milli-Q (hereafter MQ) water at room temperature in a class 100 laboratory to
179 remove any contaminants from the outer edges of the core, placed in a sealable
180 polyethylene bag and immediately stored frozen ($-34\text{ }^\circ\text{C}$) to ensure that the sample did
181 not melt prior to analysis.

182

183 Due to sample volume limitations resulting from previous studies of the Dasuopu core
184 (e.g. Thompson et al., 2000; Davis et al., 2005), 52 firn samples (5.5 - 10 cm length)
185 were collected at discontinuous intervals (where sufficient sample volume was
186 available) from 8.4 - 56.4 m depth in the cold room ($-5\text{ }^\circ\text{C}$) using a band saw. The outer

187 2 cm of each sample (n = 56) was removed using clean stainless-steel knives (soaked
188 in 2 N HNO₃ and rinsed with MQ water) under laminar flow conditions in the cold room
189 to remove surface contaminants. Clean firn samples were stored frozen (-30 °C) in
190 double polypropylene bags until analysis.

191

192 **2.3 BC analysis**

193 rBC was quantified by laser induced incandescence using a Single Particle Soot
194 Photometer (SP2; Droplet Measurement Technologies, Longmont, U.S.A.; Schwarz et
195 al., 2006; Wendl et al., 2014) at Central Washington University (Ellensburg, WA, USA).
196 Frozen samples were melted at room temperature, transferred from storage bags into
197 50 ml polypropylene centrifuge tubes, and sonicated for 20 minutes immediately prior to
198 analysis. Each liquid sample was stirred with a magnetic bar as water was routed into a
199 CETAC U-5000AT+ ultrasonic nebulizer (Teledyne CETAC Technologies, Omaha,
200 U.S.A.; ~18% nebulization efficiency at 220 nm, 356 nm, and 505 nm particle size
201 (Menking, 2013, Wendl et al., 2014)) using a peristaltic pump. The resultant aerosols
202 flowed to the SP2 inlet at a known rate using carbon-free air carrier gas. The peak
203 intensity of light emitted by an incandescing rBC particle is linearly proportional to its
204 mass (Schwarz et al., 2006), and the SP2 detects this emitted light using the amplified
205 output from 2 photodetectors (broadband and narrowband) to provide a detection range
206 of ~70 – 500 nm volume-equivalent-diameter (VED; Kaspari et al., 2014). A 5-point
207 calibration curve (~0.75 – 12.5 ppb) using Aquadag standards and MQ water was
208 performed daily to correct for BC loss during nebulization (Wendl et al., 2014). MQ
209 water was analyzed every 5 samples as a blank to monitor instrument baseline
210 conditions. If the baseline was above background levels, then MQ water would be run
211 through the system until stability was achieved. Baseline instability was not observed
212 throughout the course of the analysis. The SP2 data output was processed using the
213 PSI SP2 Toolkit ver. 4.100a (Paul Scherrer Institut, CH) and the IGOR Pro software
214 platform (WaveMetrics Inc., Portland, U.S.A.).

215

216 **2.4 Spectral analysis**

217 The record of rBC concentration with depth through the Dasuopu ice core provides a
218 time series of rBC deposition onto Dasuopu glacier over time. The decomposition of the
219 time series into time-frequency space using spectral analysis (wavelet analysis) permits
220 the identification of dominant modes of variability and their variance with time (Torrence
221 and Compo, 1998). Wavelet analysis is well suited to the analysis of time series data
222 where frequency and/or magnitude is non-stationary through the signal (Debret et al.,
223 2007). For example, wavelet analyses have been used to identify Himalayan climatic
224 oscillations related to orbital forcing, Dansgaard-Oeschger cycles, and Heinrich events
225 in the 1992 Guliya ice core (Yang et al., 2006), characterize the increased role of ENSO
226 climate forcing on Antarctic temperature since ~1850 from ice core records from East
227 and West Antarctica (Rahaman et al., 2019), and a switch from external forcing to
228 internal forcing mechanisms on global climate during the mid-Holocene (Debret et al.,
229 2009).

230

231 The ice core sampling strategy employed here may influence the results of the spectral
232 analysis because the uppermost firn section was not sampled continuously and there
233 are occasional sampling gaps in the glacier ice section (Suppl. Info. Table 1). The
234 discontinuous sampling of the firn section likely resulted in an incomplete
235 characterization of the rBC deposited onto the Dasuopu glacier since 1944 (56.4 m
236 depth). Further, the number of samples per year is not consistent throughout the record
237 because of interannual differences in snow accumulation (Suppl. Info. Fig. 1). It is
238 important to note that the spectral analysis treats the rBC time series as a linear depth-
239 time function. However, because the depth-time relationship in the ice core is not linear,
240 data is treated here as a function of the sample number of progression with depth in the
241 ice core, while the dates of the individual features detected relative to sample number
242 are specified using the Thompson et al. (2000) depth-age model. Therefore, the
243 spectral decomposition of the time series into time-frequency space is achieved while
244 minimizing the influence of data gaps and non-linear accumulation rate.

245

246 The wavelet analysis of the Dasuopu rBC record was performed using the Wavelet
247 Toolbox in Matlab (ver. R2020a; Mathworks). A continuous 1-D wavelet transform was

248 generated to identify modes of variability and the characteristics of that variability with
249 time throughout the rBC record. The Mexican Hat (or Rickler) mother wavelet was
250 chosen because it is similar to the shape of the annual variability in the rBC
251 concentration signal across the time series (Suppl. Info. Fig. 2).

252

253

254 **2.5 Trace element analysis**

255 Trace element quantification at equivalent depths as the rBC was only possible for the
256 glacier ice section of the Dasuopu ice core due to lack of sampling volume in the
257 corresponding overlying firn sections. Trace element concentration was determined by
258 Inductively Coupled Plasma Sector Field Mass Spectrometry (ICP-SFMS) at BPCRC.
259 Twenty three trace elements were measured (Al, As, Ba, Bi, Cd, Co, Cr, Cs, Fe, Ga,
260 Mg, Mn, Mo, Nb, Ni, Pb, Rb, Sb, Ti, Tl, U, V, and Zn) using methods described in
261 Uglietti et al. (2014) and reported by Gabrielli et al. (2020). The trace element crustal
262 enrichment factor (EF) is used to identify trace element contributions exceeding natural
263 background levels, and was calculated relative to Fe and elemental ratios of dust from
264 the Tibetan Plateau following Gabrielli et al. (2020) as an additional variable to be
265 compared with rBC.

266

267 **2.6 Back trajectory analysis**

268 While the complex topography of the Himalayas affects local wind patterns, back
269 trajectory modeling permits the characterization of the broader regional catchment from
270 which rBC may be derived. Atmospheric circulation capable of delivering rBC to
271 Dasuopu glacier was identified using the Hybrid Single Particle Lagrangian Trajectory
272 Model (HSYPLIT; NOAA Air Resources Laboratory, 2018). A 7-day back trajectory was
273 chosen as a conservative estimate of rBC atmospheric residence time given the range
274 reported in the literature (e.g. Ogren and Charlson, 1983; Reddy and Boucher, 2004,
275 2007; Samset et al., 2014; Lund et al., 2018). Back trajectories from the Dasuopu drill
276 site were calculated at 6 hour intervals from 1948-1991 for January (winter/non-
277 monsoon) and July (summer/monsoon) using the NCEP/NCAR (National Centers for

278 Environmental Prediction/National Center for Atmospheric Research) reanalysis from
279 1948 (the limit of the NCEP/NCAR dataset) to 1991.

280

281 **3 Results**

282 **3.1 The rBC record**

283 Figure 2a shows the 211-year rBC record from the Dasuopu ice core. The mean rBC
284 concentration is 1.5 $\mu\text{g/L}$ (SD = 5.0, n = 1628) from 1781 (± 3 years) to 1992 CE. The
285 mean rBC concentration in the glacier ice section from 1781 to 1944 and the
286 discontinuously sampled firn section from 1944 to 1992 is 1.4 $\mu\text{g/L}$ (SD = 4.4, n = 1572)
287 and 6.0 $\mu\text{g/L}$ (SD = 13.5, n = 52), respectively. Note that the median values for the
288 same time periods are less influenced by outliers with high concentrations (median
289 1781 to 1944 = 0.2 $\mu\text{g/L}$, 1944 to 1992 = 0.6 $\mu\text{g/L}$). Even though the rBC concentration
290 in the ice and firn described here is significantly different (two tailed Mann-Whitney U
291 test, $p < 0.05$), the effect of discontinuously sampling the firn section and its accurate
292 characterization of rBC since 1944 is unknown. It is possible that the firn section is
293 biased towards higher rBC concentrations because only 13% (7 of 52) of the firn
294 samples correspond to snow deposited during monsoon conditions, as indicated by
295 depleted $\delta^{18}\text{O}$ (Suppl. Fig. 4), that is a period associated with lower atmospheric aerosol
296 loading (Lelieveld et al., 2018). In general, increases in rBC concentration corresponds
297 to $\delta^{18}\text{O}$ enrichment (Fig. 3) and increased dust in glacier ice, indicating that higher rBC
298 concentrations coincide with the non-monsoonal dry season (Fig. 3, Suppl. Fig 4 for firn
299 section; Kaspari et al., 2014). Occasional exceptions occur, for example in 1824 CE,
300 when a period of high rBC concentrations corresponds to a relatively low dust
301 concentration and a low $\delta^{18}\text{O}$ value (Fig. 3a). The relationship is between $\delta^{18}\text{O}$
302 enrichment and rBC over a broader and continuous time window is show in Fig. 3d.
303 Here, an analysis of the magnitude-squared coherence between 1856 – 1943 is shown
304 at scales ranging from a single rBC measurement (period = 1) to 953 rBC
305 measurements (period = 476 data points) shows high coherence at longer periods
306 (>256 data points) with no phase lag (as indicated by horizontal arrows orientated to the
307 right), strong coherence between 1878 – 1900 CE at a period of 24 – 120 data points
308 (~2 -10 years; 1 year = 12 data points (Suppl Fig. 1)) with a lag in rBC of 0.25 of a cycle

309 (as indicated by the vertical arrow), or 0.25 – 2.5 years (6 – 30 data points), suggesting
310 that rBC increases on the end of the dry season during this period. There is also a band
311 of strong coherence from 1910 - 1943 occurring with a periodicity of ~15 years (~ 8
312 points per year (Suppl. Fig. 1)) with no phase lag suggesting that rBC concentrations
313 reach their maximum at the peak of the dry season.

314
315 The smoothed (5 year median) rBC concentration and flux (the product of mean annual
316 rBC concentration and snow accumulation) records show an increase beginning in
317 ~1870 and again in ~1935 (Fig. 2a, b). The discontinuous firn section of the core has
318 elevated concentrations during the late 1960s - 1970s, consistent with observations
319 from East Rongbuk glacier by Ming et al. (2008) and Kaspari et al. (2011), and for
320 Tanggula glacier by Xu et al. (2009).

321

322 **3.2 Spectral Analysis**

323 We chose to examine 3 modes of variability within the spectral analysis (Fig. 4b), 2 of
324 which correspond to North Atlantic sea surface temperature (SST) because of the
325 important role of westerly atmospheric circulation in the Dasuopu region during the
326 winter non-monsoonal season (Davis et al., 2005); the annual frequency that is that is
327 responsible for 90% of the variance in the seasonal cycle of SST in the North Atlantic
328 (Feliks et al., 2011), and ~4.5 year variability that is the middle value of 3 modes of SST
329 oscillation (3.7, 4.5, and 6.2 years; Feliks et al., 2011) in the Cape Hatteras region of the
330 North Atlantic (44 °N, 47 °W). A third mode of variability (~85 years) was chosen to
331 identify longer-term variation in the rBC record.

332 The mode at $a = 6$ ($a = 0.5 \times \text{frequency}$) indicates high frequency, and generally,
333 relatively low amplitude variability in spectral coefficients (81% of rBC concentrations
334 are $< 1 \mu\text{g/L}$) occurring at ~ annual (12 data points/year; $\text{SD} = 4.3$, $n = 112$) resolution
335 with isolated relatively higher amplitude events dispersed throughout the record (Fig.
336 4c). The frequency of these higher amplitude events increases from ~1877 until 1992
337 CE (Fig. 4a, c).

338 The lower frequency mode ($a = 27$; ~4.5 years) captures periodic peaks in rBC
339 concentrations centered at 1825, 1877, 1888, 1908, 1920, 1930, and 1977 CE if peaks

340 that are >25% of the largest peak's amplitude in the time series (1977 CE) are
341 considered (Fig. 4d). Dips in the $a = 27$ spectral coefficients indicating periods of low
342 amplitude (defined here as >25% of the amplitude of the lowest dip at 1937 CE), occur
343 at 1818, 1868, 1875, 1880 - 1884, 1893, 1914, 1924, and 1937 CE (Fig. 4d).

344 The $a = 512$ (~85 year) mode identifies a shift from some samples with negative
345 spectral coefficients (values below zero) to those with positive spectral coefficients at
346 ~1877 CE (Fig. 4e). All three modes identify a period early in the rBC record
347 characterized as a quiescent period (1781 - 1877 CE) where rBC concentrations do not
348 exceed $19.3 \mu\text{g/L}$ (mean = 0.8, SD = 3.0, $n = 880$), except for the isolated peak (63.3
349 $\mu\text{g/L}$) at 1825 CE (Fig. 4a, c, d)). Prior to 1877 the rBC concentration in the ice core is
350 significantly lower (Mann-Whitney U test, $p < 0.05$) and less variable (mean = 0.8, SD =
351 3.03, $n = 898$) than the post 1877 period (mean = 2.3, SD = 6.6, $n = 732$; Fig. 4). While
352 the ~85 year mode identifies a shift from negative to positive spectral coefficients in
353 1877, the 5 year median of the rBC record identifies an increase occurring at ~1870.
354 This suggests that the wavelet analysis may be sensitive to individual or tightly
355 clustered peaks in the rBC record, such as those that occur between 1875 and 1880
356 (Fig. 3a, 4a).

357

358 **3.3 Comparison of the rBC record with the trace element record**

359 When considering the full record ($n = 857$ to 916 depending on the element; Table 1), all
360 of the trace element concentrations analyzed are significantly correlated with rBC
361 (range of 0.15 (Zn; $n = 915$) to 0.27 (Rb; $n = 914$); Table 1; $\alpha = 0.01$; Spearman
362 correlation test is used instead of Pearson correlation test because the rBC and trace
363 element data are not normally distributed). If the low-rBC pre-1877 period, as indicated
364 by the spectral analysis, is considered independently, then the correlation between
365 trace element and rBC are still statistically correlated (range of 0.26 (Zn, $n = 915$) to
366 0.44 (Mg and Mn, $n = 915$). In contrast, the post 1877 period shows a statistically
367 insignificant slightly negative correlation between the trace elements and rBC ranging
368 from -0.04 (Cs and Nb, $n = 913$ and 915, respectively) to -0.10 (Bi and Mn, $n = 857$ and
369 915, respectively).

370

371 The crustal enrichment factor (EF) for all of the trace elements were significantly weakly
372 to moderately negatively correlated with rBC for all trace elements, ranging from -0.21
373 for Mg to -0.57 for Ga, except for Mn which was insignificantly positively correlated
374 (0.02). The trace element EFs were more negatively correlated to rBC during the post
375 1877 period than the pre-1877 period (excluding Mn because it was insignificantly
376 correlated; SD = 0.14), although this difference is not statistically significant, $t(22) =$
377 1.88, $p = 0.07$ ($p < 0.05$).

378

379 **3.4 Back trajectory**

380 Figure 5a shows the results of the July back trajectory showing that aerosols are
381 primarily derived from areas to the south-west of the Dasuopu drill site, from the Arabian
382 Sea and across western and northern India during the monsoon. A secondary source is
383 located to the west and draws atmospheric aerosols from the eastern Mediterranean
384 Sea and Arabian Peninsula. January (non-monsoon) circulation is derived from the
385 westerly circulation across north-eastern Africa, Central Europe, the Arabian Peninsula
386 and north-west India (Fig. 5b).

387

388 **4 Discussion**

389 **4.1 rBC concentrations**

390 The mean rBC concentration in the Dasuopu ice core, from 1781 to 1992 CE is 1.5 $\mu\text{g/L}$
391 (SD=5.0, n=1628); 6 times higher than the average rBC reported by Kaspari et al.
392 (2011) for the period 1860-1992 and ~2 times lower than BC reported by Ming et al.
393 (2008) and Xu et al. (2008) for the East Rongbuk ice core record over similar time
394 periods (Fig. 1). Note that while Kaspari et al. (2011) measured BC from the East
395 Rongbuk core using the same incandescence method used here, samples were stored
396 as liquid and measured concentrations are likely underestimated due to rBC particle
397 adherence onto the walls of the storage container and/or agglomeration of BC particles
398 above the detected particle size range (Wendl et al., 2014; Kaspari et al., 2014). In
399 contrast, Ming et al. (2008) and Xu et al. (2009) measured BC concentration by thermo-
400 optical methods, which may result in an overestimation of reported BC due to organic

401 matter pyrolysis during analysis (Gilardoni and Fuzzi, 2017), and a larger fraction of the
402 carbonaceous particles being classified as BC.

403

404 **4.2 rBC seasonality**

405 Seasonally, peaks in rBC concentration correspond to intervals of increased dust
406 concentration and enriched $\delta^{18}\text{O}$ over the entire ice core record (see examples in Fig.
407 3), indicating high BC concentrations are associated with the non-monsoonal season
408 when drier westerly air masses dominate atmospheric circulation (Fig. 5). Weather
409 station measurements and previous snow/ice studies in the region confirm that rBC
410 concentrations are lower in near-surface air at the Nepal Climate Observatory-Pyramid
411 (NCO-P; 5079 m a.s.l.) during the monsoon (Bonasoni et al., 2010; Marinoni et al.,
412 2010, 2013) and higher during the pre-monsoon period (Babu et al., 2011; Nair et al.,
413 2013; Ginot et al., 2014; Kaspari et al., 2014; Chen et al., 2018).

414

415 **4.3 Temporal variations in high rBC concentrations and regional climate**

416 The pre-1877 CE period differs from the post-1877 CE period in the frequency and
417 amplitude of variability in rBC concentration (Fig. 2a and 4e). The high rBC
418 concentration event in ~1825 CE (Fig. 4c) occurs during an otherwise quiescent pre-
419 1877 CE period coinciding with a time of severe regional moisture stress/droughts as
420 reflected in suppressed tree ring growth across Nepal, peaking in 1817 CE (Figs. 6 and
421 7 in Thapa et al., 2017). This period of abnormally dry conditions occurs after 2 large
422 volcanic events; the Tambora eruption of 1815 (Stothers, 1984) and an eruption of
423 unknown origin in 1809 CE (Cole-Dai et al., 2009). Anchukaitis et al. (2010) argue that
424 major explosive eruptions in the tropics can disrupt the Asian monsoon system and
425 result in drier conditions in central Asia for up to 8 years afterward. Dry conditions are
426 typically associated with an increase in the frequency and severity of biomass burning in
427 south-east Asia (Baker and Bunyavejchewin, 2009) and the association between dry
428 conditions and increases in rBC concentration suggests that biomass burning may be a
429 source of high rBC concentration events at Dasuopu glacier.

430

431 From ~1877 CE until the end of the rBC record in 1992, rBC concentrations are
432 significantly higher and their amplitude increases, as indicated by the shift from negative
433 to positive spectral coefficients at $a = 512$ (Fig. 4e). This suggests a change in either the
434 magnitude of rBC emission source(s) or in the atmospheric mechanism that delivers
435 rBC to Dasuopu glacier after ~1877 CE. The post ~1877 increase in rBC corresponds to
436 a decrease in snow accumulation onto Dasuopu glacier (Fig. 2c; Davis et al., 2005) and
437 an increase in the rBC flux from the atmosphere beginning in ~1880 (Fig. 2b). This
438 decrease in snow accumulation has been linked to a strengthening of the Icelandic Low
439 pressure system as temperatures in the Northern Hemisphere warmed at the
440 termination of the Little Ice Age (LIA). This resulted in a shift in the North Atlantic
441 Oscillation Index (NAO) from a negative mode to a positive mode, contributing less
442 moisture to the southern Himalaya during winter (Davis et al., 2005). Less winter snow
443 accumulation post ~1877 would be associated with drier winter (non-monsoon)
444 conditions generally, when rBC concentration is highest at Dasuopu glacier.

445

446 **4.4 The influence of drought and biomass burning on the rBC record**

447 Biomass burning, and associated rBC emissions result from dry conditions and drought
448 that lowers the water table and dries biomass fuel (Baker and Bunyavejchewin, 2009;
449 Tosca et al., 2010). Further, aerosols produced during fires may contribute to a positive
450 feedback cycle where smoke plume shading decreases sea surface temperature, while
451 increased concentrations of atmospheric BC warm and stabilize the troposphere,
452 suppressing convection and precipitation and intensifying drought conditions on land
453 (Tosca et al., 2010). High BC aerosol levels in ambient air corresponding to agricultural
454 burning beginning in late April and forest fire activity during the non-monsoon season
455 was reported by Negi and others (2019) from ambient air measurements at Chirbasa,
456 India (Gangotri glacier valley) during 2016. The spectral coefficients calculated here
457 identify trends in rBC concentration onto Dasuopu glacier and can be compared to
458 regional rainfall data from a network of rain gauge stations that are distributed across
459 India to identify periods of dryness (e.g., Parthasarathy et al. 1987) associated with
460 higher rBC concentrations.

461

462 Continuous regional instrumental rainfall records within the atmospheric catchment for
463 atmospheric aerosols to Dasuopu glacier prior to the early 1900s CE are rare, and
464 biomass burning records are non-existent. However, continuous tree ring-based
465 reconstructions of precipitation conditions for Europe, North Africa, and the Middle East
466 is provided by the Old World Drought Atlas (OWDA; Cook et al., 2015) and includes
467 areas identified by the back trajectory analysis as being potential source regions for rBC
468 to Dasuopu glacier (Fig. 5b). The Monsoon Asia Drought Atlas (MADA; Cook et al.,
469 2010) provides a similar dataset for regions in East Asia, including Pakistan and
470 Afghanistan, which may contribute rBC to Dasuopu glacier (Fig. 5b). An instrumental
471 record for both the OWDA and MADA begins in 1901 (Fig. 6). Comparing the peaks in
472 rBC concentration identified by the spectral coefficients ($a = 27$, ~4.5 year frequency)
473 centered at 1825, 1877, 1888, 1898, 1908, 1920, 1930, and 1977 CE (Fig. 4d) to the
474 reconstructed and instrumental self-calibrating Palmer Drought Severity Index (scPDSI)
475 for the summer season (where positive and negative scPDSI indicate wet and dry
476 conditions respectively; Fig. 6), it is possible to identify periods of dryness that might
477 contribute to the production of rBC by biomass burning.

478
479 rBC wavelet coefficient peaks in 1825 and 1877 CE occur at the end of a decade-long
480 period of negative scPDSI in the OWDA and MADA reconstructions, respectively (Fig.
481 6). Similarly, 1888, 1898, and 1930 follow years of negative scPDSI in either the OWDA
482 or MADA reconstructions, indicating periods of dryness preceding episodes of elevated
483 rBC concentration at Dasuopu glacier (Fig. 6). The 1908 and 1920 CE peaks do not
484 follow periods of negative scPDSI in the OWDA or MADA reconstructions, but follows
485 periods of negative scPDSI in the MADA instrumental record (Fig. 6) indicating that
486 dryness is associated with these rBC concentration peaks as well. The peak centered at
487 1977 CE follows periods of positive scPDSI in the OWDA and MADA reconstructions
488 and instrumental records and does not appear to be related to abnormally dry
489 conditions, and may indicate an unidentified source of rBC. Conversely, dips in the
490 spectral coefficients at a ~4.5 year frequency ($a = 27$) indicate periods of low rBC
491 concentration occurring at 1818, 1868, 1875, 1880-1884, 1893, 1914, 1924, and 1936
492 CE. With the exception of the dip centered at 1875 and 1936 CE, dips in the spectral

493 coefficient record follow periods of positive scPDSI in either or both the OWDA and
494 MADA tree ring reconstruction. While dips centered at 1914 and 1924 CE follow periods
495 of positive scPDSI in both the OWDA and MADA instrumental record, 1936 CE follows
496 a period of positive scPDSI in the MADA instrumental record only (Fig. 6).

497

498 In addition to the scPDSI from OWDA and MADA tree ring reconstructions and the
499 instrumental record (since 1900 CE), an independent historical record for rainfall is
500 available for India that was compiled by Mooley et al. (1981) and has since been
501 reported in terms of drought/flood severity by Parthasarathy et al. (1987; Suppl. Table
502 1a, b). As mentioned, several periods of high rBC concentration are identified by the
503 spectral coefficients at $a = 27$ (~4.5 year frequency) centered at 1825, 1877, 1888,
504 1898, 1908, 1920, 1930, and 1977 CE (Fig. 4d). These periods of high rBC
505 concentration coincide with periods of drought reported for India, particularly in
506 western/northwestern meteorological subdivisions (Parthasarathy et al., 1987) within the
507 ± 3 years dating error of the ice core chronology (Fig. 7; Suppl. Fig. 3 a). For example,
508 from 1876 – 1878, India experienced widespread moderate to severe drought
509 conditions (Parthasarathy et al., 1987; Fig. 7a) and soil moisture deficits (Mishra et al.,
510 2019) that resulted in the “Madras Famine” (Cook et al., 2010; Mishra et al., 2019). In
511 1888 (and 1891 which is within the ± 3 year ice core dating uncertainty), regions in
512 western and northwestern India experienced moderate and severe drought conditions
513 (Fig. 7b). In 1899 (corresponding to 1898 in the rBC record, ± 3 years), northwest and
514 western meteorological subdivisions (among others) experienced severe drought while
515 moderate drought was experienced by most of India (Fig. 7c), resulting in famine that
516 affected 59.5 million people (Mishra et al., 2019). In 1911 (1908 ± 3 years) there was
517 extreme drought reported in the northwest and moderate drought reported in the north-
518 central and southwest meteorological districts (Fig. 7d). In 1918 (1920 ± 3 years), there
519 was severe drought reported in the north and central-west and moderate drought
520 reported throughout the south and north-central regions of the continent (Fig. 7e). From
521 1927-1929 (1930 ± 3 years), moderate drought was reported in the northern region of
522 India (Fig. 7f). Similar to observations from the OWDA and MADA comparisons, the
523 ~1977 period does not stand out in the climate record as being exceptional (Suppl. Fig.

524 3), and it does not correspond to anomalously high rBC values (Fig. 2a) yet it
525 corresponds with a period of highly positive spectral coefficients (Fig. 4c, d). Finite-
526 length signal border effects (so called edge effects) have been well documented, where
527 a wavelet transform (such as that used here) yield abnormal coefficients as the wavelet
528 extends into the “shoulder areas” of the record that don’t have data (Su et al., 2011,
529 Montanari et al., 2015). It is possible that the peak identified here at $a = 6$ and $a = 27$ is
530 a result of wavelet transform edge effects. Alternatively, sources other than biomass
531 burning, that have not been identified here, may contribute to high rBC values observed
532 in the Dasuopu ice core ~1977 CE.

533

534 Dips in the $a = 27$ spectral coefficient record correspond to periods of flooding in India.
535 For example, the trough at 1875 CE corresponds to reports of extreme flooding in the
536 north-west and moderate flooding in western India (Fig. 8a). It should be noted that
537 moderate drought was reported in the far west and south, but these conditions did not
538 result in a rBC peak in the $a = 27$ coefficients (Fig. 4d). For the period ~1880 to 1886
539 CE, severe and moderate flooding is reported in the west in 1884 CE, with moderate
540 drought to the south and east that did not result in an rBC peak in the $a = 27$ coefficients
541 (Fig. 8b). From 1880 – 1882 CE, the continent experienced relatively stable conditions
542 with moderate flooding in some western and north-western districts (Suppl. Info. Fig. 3).
543 Western India experienced severe and moderate flooding in the west and northwest in
544 1893 (Fig. 8c), corresponding to a dip in the $a = 27$ coefficients (Fig. 4d). 1914 and 1917
545 (1914 ± 3 years), 1926 (1924 ± 3 years) and 1933 (1936 ± 3 years) all saw severe
546 and/or moderate flooding in western meteorological districts, with no drought conditions
547 reported in the rest of India, corresponding to dips in the $a = 27$ coefficients (Fig. 8d, e, f
548 respectively).

549

550 **4.5 rBC and trace metals**

551 Recent work by Gabrielli and others (2020) suggested that atmospheric trace metals
552 preserved in the Dasuopu ice core, likely linked to the long-range transport of fine fly
553 ash, were indicative of emissions from coal combustion and fires used to clear forested
554 areas to the west of the Himalayas since the beginning of the Industrial Revolution

555 (~1780 CE). Fly ash is composed of alumino-silicate and iron-rich byproducts of coal
556 combustion and biomass burning and is enriched in trace metals (Ross et al., 2002). Fly
557 ash is not detected by the SP2 as configured here.

558

559 We observe a general negative correlation between BC and the crustal enrichment
560 factor (EF; indicative of element concentrations above the natural background derived
561 from crustal material) of trace metals in the Dasuopu core, particularly after 1877 CE
562 (Table 1) when rBC spectral coefficients are positive at $a = 512$ (Fig. 4e). This illustrates
563 that the enrichment of the non-crustal fraction of trace metals (as indicated by a positive
564 EF), and fly ash, occurred out of phase from rBC.

565

566 Increases in the concentration of rBC resulting from biomass burning may be expected
567 to correlate with trace elements associated with the biomass source material (K, Cl, Zn,
568 and Br; Echalar et al., 1995). Of these, only Zn was analyzed here. Zn concentration is
569 only weakly correlated with rBC (0.15), although more strongly (0.26) in the pre-1877
570 period than in the post-1877 period (-0.06), and Zn's EF is moderately negatively
571 correlated, particularly in the post 1877 period (-0.63). While the lack of correlation
572 between potential biomass burning-derived trace elements such as Zn and rBC might
573 suggest a non-biomass burning source for rBC, one should be cautious in attributing
574 specific trace elements to biomass burning events. For example, trace elements emitted
575 during partial combustion can vary depending on fire intensity (flaming vs. smoldering),
576 fuel source (savanna vs. forest) (Echalar et al., 1995), and size-dependent particle
577 adhesion (Samsonov et al., 2012). Further, biomass burning remobilizes soil-derived
578 particles which would lower the individual trace element's EF (Gaudichet et al., 1995)
579 causing a negative correlation between rBC and EF_c. There is a statistically significant
580 negative correlation with rBC to all of the trace element EFs (except for Mn), suggesting
581 that rBC enrichment is not associated with non-crustal trace element enrichment,
582 interpreted as an indicator of fly ash deposition (Gabrielli et al., 2020), that is enriched
583 above the natural dust input. Of importance is that the discontinuous sampling of firn in
584 the Dasuopu ice core record presented here does not capture a continuous record of
585 rBC deposition during the post 1970s; a period when rBC is reported to have increased

586 in the southern Himalaya (Kaspari et al., 2011) and Tibetan Plateau (Jenkins et al.,
587 2016; Wang et al., 2015).

588

589 **5 Conclusions**

590 Here, we present the highest elevation (7200 m asl) record of rBC ever reported. This
591 record is unique in its high elevation and represents conditions in the free troposphere,
592 away from local sources of BC. The Dasuopu record also contributes to the limited
593 number of proxy records of BC in the HKH region where glacier melt, and therefore
594 factors such as BC that affect glacier melt, influence the water security of one of the
595 most densely populated regions of the planet. While the Dasuopu rBC record presented
596 here is not well resolved during the period after the 1970s, the record does indicate
597 elevated BC during 1970-1980, consistent with the Everest ice core BC record that
598 showed elevated BC post 1970 (Kaspari et al., 2011).

599

600 rBC concentration at the Dasuopu site is highest during the winter (non-monsoon)
601 season when westerly circulation is dominant. Back trajectory analyses indicate that this
602 westerly circulation predominantly includes areas of west/northwest India, Afghanistan,
603 Pakistan, northern Africa, central Europe and the Mediterranean. Dry conditions
604 increase the production of rBC through biomass burning and we suggest that regional
605 biomass burning contributes to periods of high rBC deposition onto the Dasuopu glacier
606 during periods of dryness as indicated by historical records of precipitation within the
607 atmospheric catchment of Dasuopu glacier. The continuous historical record of
608 precipitation for India, in particular, suggests an association between moderate to
609 severe drought conditions in west/north-west India and rBC concentration in the
610 Dasuopu ice core. Upwind industrial sources of rBC, such as coal combustion, appear
611 to be of minor influence during these periods of increased rBC deposition as indicated
612 by the absence of correlation between rBC concentration in the Dasuopu core and the
613 crustal enrichment of industrially-sourced trace elements at equivalent depths in the ice
614 core. It should be noted that the Dasuopu ice core rBC record is discontinuous during
615 the period of increased regional industrial activity thus the available data cannot
616 address the importance of this regional industrialization to rBC deposition onto Dasuopu

617 glacier. Together, evidence presented here indicates that while rBC transport in the free
618 troposphere is influenced by large scale synoptic circulation, regional sources of rBC
619 strongly influence rBC deposition onto Dasuopu glacier, particularly after ~1877, and
620 that the rBC record from Dasuopu glacier may provide a proxy record for drought and
621 resultant biomass burning within its catchment of atmospheric circulation.

622

623 **Acknowledgments**

624 This work was funded by the NSF Atmospheric Chemistry Program (award # 1149239)
625 and the by the NSF-ESH program, The Ohio State University, the Ohio State
626 Committee of Science and Technology, and the National Natural Science Foundation of
627 China. We thank the many scientists, engineers, technicians, and graduate students
628 from the Byrd Polar and Climate Research Center and the Lanzhou Institute of
629 Glaciology and Geocryology (China) that contributed to the collection and previous
630 analysis of the Dasuopu ice core. We are grateful to Julien Nicolas for performing the
631 graphic display of the back trajectories. This is BPCRC contribution no. xxxx.

632

633 **Data availability**

634 The data presented in this work are archived at the National Oceanic and Atmospheric
635 Administration World Data Center-A for Paleoclimatology at xxxx.

636

637 **Author contribution**

638 Barker performed the sample preparation, BC analysis and interpretation, and was the
639 primary author of the manuscript. Kaspari assisted with the BC analysis and
640 interpretation of the BC record. Gabrielli designed the overall project, performed the
641 trace element analysis with Wegner. Wegner, Beaudon, and Sierra-Hernández cut the
642 samples from the ice core and performed the trace element analysis. Thompson
643 retrieved the Dasuopu ice core. All authors contributed to manuscript preparation.

644

645 **Competing interests**

646 The authors declare that they have no conflict of interest.

647

648 **References**

- 649 Anchukaitis, K.J., Buckley, B.M., Cook, E.R., D'Arrigo, R.D., and Ammann, C.M.:
650 Influence of volcanic eruptions on the climate of the Asian monsoon region,
651 *Geophys. Res. Lett.*, 37, 1-5, doi: 10.1029/2010GL044843, 2010.
- 652 Babu, S.S., Chaubey, J.P., Moorthy, K.K., Gogoi, M.M., Kompalli, K.K., Sreekanth, V.,
653 Bagare, S.P., Bhatt, B.C., Gaur, V.K., Prabhu, T.P., and Singh, N.S.: High
654 altitude (~4520 m amsl) measurements of black carbon aerosols over western
655 trans-Himalayas: Seasonal heterogeneity and source apportionment, *J.*
656 *Geophys. Res.-Atmos.*, 116, D24201, doi: 10.1029/2011JD06722, 2011.
- 657 Baker, P.J., and Bunyavejchewin, S.: Fire behavior and fire effects across the forest
658 landscape of continental Southeast Asia. In: *Tropical Fire Ecology*. Springer
659 Praxis Books. Springer, Berlin, Heidelberg, doi: 10.1007/978-3-540-77381-8_11,
660 2009.
- 661 Bonasoni, P., Laj, P., Marinoni, A., Sprenger, M., Angelini, F., Arduini, J., Bonafe, U.,
662 Calzolari, F., Colombo, T., Decesari, S., Di Biagio, C., di Sarra, A.G., Evangelisti,
663 F., Duchi, R., Facchini, MC., Fuzzi, S., Gobbi, G.P., Maione, M., Panday, A.,
664 Roccatò, F., Sellegri, K., Venzac, H., Verza, GP., Villani, P., Vuillermoz, E., and
665 Cristofanelli, P.: Atmospheric brown clouds in the Himalayas: first two years of
666 continuous observations at the Nepal Climate Observatory-Pyramid (5079 m),
667 *Atmos. Chem. Phys.*, 10, 7515-7531, doi: 10.5194/acp-10-7515-2010, 2010.
- 668 Bond, T.C., Streets, D.G., Yarber, K.F., Nelson, S.M., Woo, J.-H., and Klimont, Z.: A
669 technology-based global inventory of black and organic carbon emissions from
670 combustion, *J. Geophys. Res. Atmos.*, 109, D14, doi: 10.1029/2003JD003697,
671 2004.
- 672 Bond, T.C., Bhardwaj, E., Dong, R., Jogani, R., Jung, S., Roden, C., Streets, D.G., and
673 Trautmann, N.M.: Historical emissions of black and organic carbon aerosol from
674 energy-related combustion, 1850-2000, *Global Biogeochem. Cy.*, 21, GB2018,
675 doi: 10.1029/2006GB002840, 2007.
- 676 Bond, T.C., Doherty, S.J., Fahey, D.W., Forster, P.M., Bernsten, T., DeAngelo, B.J.,
677 Flanner, M.G., Ghan, S., Karcher, B., Koch, D., Kinne, S., Kondo, Y., Quinn,
678 P.K., Sarofim, M.C., Schultz, M.G., Shulz, M., Venkataraman, C., Zhang, H.,
679 Zhang, S., Bellouin, N., Guttikunda, S.K., Hopke, P.K., Jaconson, M.Z., Kaiser,
680 J.W., Klimont, Z., Lohmann, U., Schwarz, J.P., Shindell, D., Storelvmo, T.,
681 Warren, S.G. and Zender, C.S.: Bounding the role of black carbon in the climate
682 system: A scientific assessment, *J. Geophys. Res.-Atmos.*, 118, 5380-5552, doi:
683 10.1002/jgrd.50171, 2013.
- 684 Cao, J., Tie, X., Xu, B., Zhao, Z., Zhu, C., Li, G., and Liu, S.: Measuring and modeling
685 black carbon (BC) contamination in the SE Tibetan Plateau, *J. Atmos. Chem.*,
686 67, 45-60, doi: 10.1007/s10874-011-9202-5, 2010.
- 687 Chaubey, J.P., Babu, S.S., Gogoi, M.M., Kompalli, S.K., Sreekanth, V., Moorthy, K.K.,
688 and Prabhu, T.P.: Black carbon aerosol over a high altitude (~ 4.52 km) station in
689 Western Indian Himalayas, *J. Inst. Eng.*, 8, 42-51, doi: 10.3126/jie.v8i3.5930,
690 2011.
- 691 Chen, X., Kang, S., Cong, Z., Yang, J., and Ma, Y.: Concentration, temporal variation

692 and sources of black carbon in the Mount Everest region retrieved by real-time
693 observation and simulation, *Atmos. Chem. Phys.*, 18, 12859-12875, doi:
694 10.5194/acp-18-12859-2018, 2018.

695 Cole-Dai, J., Ferris, D., Lanciki, A., Savarino, J., Baroni, M., and Thiemens, M.H.: Cold
696 decade (AD 1810-1819) caused by Tambora (1815) and another (1809)
697 stratospheric volcanic eruption, *Geophys. Res. Lett.*, 36, L22703, doi:
698 10.1029/2009GL040882, 2009

699 Cook, E.R., Anchukaitis, K.J., Buckley, B.M., D'Arrigo, R.D., Jacoby, G.C., and Wright,
700 W.E.: Asian monsoon failure and megadrought during the last millennium,
701 *Science*, 328, 486-489, doi: 10.1126/science.1185188, 2010.

702 Cook, E.R., Seager, R., Kushnir, Y., Briffa, K.R., Buntgen, U., Frank, D., Krusic, P.J.,
703 Tegel, W., van der Schrier, G., Andreu-Hayles, L., Baillie, M., Baittinger, C.,
704 Bleicher, N., Bonde, N., Brown, D., Carrer, M., Cooper, R., Cufar, K., Dittmar, C.,
705 Esper, J., Griggs, C., Gunnarson, B., Gunther, B., Gutierrez, E., Haneca, K.,
706 Helama, S., Herzig, F., Heussner, K.-U., Hofmann, J., Janda, P., Kontic, R.,
707 Kose, N., Kynცი, T., Levanic, T., Linderholm, H., Manning, S., Melvin, T.M., Miles,
708 D., Neuwirth, B., Nicolussi, K., Nola, P., Panayotov, M., Popa, I., Rothe, A.,
709 Seftigen, K., Seim, A., Svarva, H., Svoboda, M., Thun, T., Timonen, M.,
710 Touchan, R., Trotsiuk, V., Trouet, V., Walder, F., Wazny, T., Wilson, R., and
711 Zang, C.: Old world megadroughts and pluvials during the Common Era, *Sci.*
712 *Adv.*, 1, doi: 10.1126/sciadv.1500561, 2015

713 Davis, M.E., Thompson, L.G., Yao, T., and Wang, N.: Forcing of the Asian monsoon on
714 the Tibetan Plateau: Evidence from high-resolution ice core and tropical coral
715 records, *J. Geophys. Res.*, 110, D04101, doi: 10.1029/2004JD004933, 2005.

716 Debret, M., Bout-Roumazelles, V., Grousset, F., Desmet, M., McManus, J.F., Massei,
717 N., Sebag, D., Petit, J.-R., Copard, Y., and Trentesaux, A.: The origin of the
718 1500-year climate cycles in Holocene North-Atlantic records, *Clim. Past Discuss.*,
719 3, 679-692, doi: 10.5194/cp-3-569-2007, 2007.

720 Debret, M., Sebag, D., Costra, X., Massei, N., Petit, J.-R., Chapron, E., and Bout-
721 Roumazelles, V.: Evidence from wavelet analysis for a mid-Holocene transition
722 in global climate forcing, *Quaternary Sci. Rev.*, 28, 2675-2688, doi:
723 10.1016/j.quascirev.2009.06.005, 2009.

724 Doherty, S.J., Grenfell, T.C., Forsström, Hagg, D.L., Brandt, R.E., and Warren, S.G.:
725 Observed vertical redistribution of black carbon and other insoluble light-
726 absorbing particles in melting snow, *J. Geophys. Res. Atmos.*, 118, 5553-5569,
727 doi: 10.1002/jgrd.50235, 2013.

728 Echalar, F., Gaudichet, A., Cachier, H., and Artaxo, P.: Aerosol emissions by tropical
729 forest and savanna biomass burning: characteristic trace elements and fluxes,
730 *Geophys. Res. Lett.*, 22, 3039-3042, doi: 10.1029/95GL03170, 1995.

731 Flanner, M. G., Zender, C. S., Randerson, J. T., and Rasch, P. J.: Present day climate
732 forcing and response from black carbon in snow, *J. Geophys. Res.*, 112,
733 D11202, doi:10.1029/2006JD008003, 2007.

734 Feliks, Y., Ghil, M., and Robertson, A.W.: The atmospheric circulation over the North
735 Atlantic as induced by the SST field, *J. Clim.*, 24, 522-542, doi:
736 10.1175/2010JCL13859.1, 2011)

737 Forster, P., Ramaswamy, V., Artaxo, P., Berntsen, T., Betts, R., Fahey, D.W., Haywood,

738 J., Lean, J., Lowe, D.C., Myhre, G., Nganga, J., Prinn, R., Raga, G., Schulz, M.,
739 and Van Dorland, R. Miller, H.L. (Ed.). (2007). Changes in Atmospheric
740 Constituents and in Radiative Forcing Chapter 2. United Kingdom: Cambridge
741 University Press.

742 Gabrielli, P., Wegner, A., Sierra Hernández, R., Beaudon, E., Davis, M., Barker, J.D.,
743 and Thompson, L.G., Early contamination of the Himalayan atmosphere from
744 coal combustion since the onset of the European Industrial Revolution (~1780
745 A.D.), *P. Natl. Acad. Sci. USA*, doi: 10.1073/pnas.1910485117, 2020.

746 Gaudichet, A., Echalar, F., Chatenet, B., Quisefit, J.P., and Malingre, G.: Trace
747 elements in tropical African savanna biomass burning aerosols, *J. Atmos. Chem.*,
748 22, 19-39, doi: 10.1007/BF00708179, 1995.

749 Gertler, C.G., Puppala, S.P., Panday, A., Stumm, D., and Shea, J.: Black carbon and
750 the Himalayan cryosphere: A review, *Atmos. Env.*, 125, 404-417, doi:
751 10.1016/j.atmosenv.2015.08.078, 2016.

752 Gilardoni, S., and Fuzzi, S.: Chemical composition of aerosols of different origin. *in*
753 Tomasi, C., Fuzzi, S., and Kokhanovsky, A. (eds): *Atmospheric Aerosols: Life*
754 *Cycles and Effects of Air Quality and Climate*. Wiley-VCH Verlag GmbH & Co.
755 KGaA, Weinheim, 183-221, doi: 10.1002/9783527336449.ch4, 2017.

756 Ginot, P., Dumont, M., Lim, S., Patris, N., Taupin, J.-D., Wagnon, P., Gilbert, A.,
757 Arnaud, Y., Marinoni, A., Bonasoni, P., and Laj, P.: A 10 year record of black
758 carbon and dust from a Mera Peak ice core (Nepal): variability and potential
759 impact on melting of Himalayan glaciers, *Cryosphere*, 8, 1479-1496, doi:
760 10.5194/tc-8-1479-2014, 2014.

761 Gregory, J.M., and Oerlemans, J.: Simulated future sea-level rise due to glacier melt
762 based on regionally and seasonally resolved temperature changes, *Nature*, 391,
763 474-476, doi: 10.1038/35119, 1998.

764 Hammes, K., Schmidt, M. W. I., Smernik, R. J., Currie, L. A., Ball, W. P., Nguyen, T. H.,
765 Louchouart, P., Houel, S., Gustafsson, Ö., Elmquist, M., Cornelissen, G.,
766 Skjemstad, J. O., Masiello, C. A., Song, J., Peng, P., Mitra, S., Dunn, J. C.,
767 Hatcher, P. G., Hockaday, W. C., Smith, D. M., Hartkopf-Fröder, C., Böhmer, A.,
768 Luer, B., Huebert, B. J., Amelung, W., Brodowski, S., Huang, L., Zhang, W.,
769 Gschwend, P. M., Flores-Cervantes, D. X., Largeau, C., Rouzaud, J., Rumpel,
770 C., Guggenberger, G., Kaiser, K., Rodionov, A., Gonzalez-Vila, F. J., Gonzalez-
771 Perez, J. A., de la Rosa, J. M., Manning, D. A. C., López-Capél, E., and Ding, L.:
772 Comparison of quantification methods to measure fire-derived (black/elemental)
773 carbon in soils and sediments using reference materials from soil, water,
774 sediment and the atmosphere, *Global Biogeochem. Cy.*, 21, GB3016,
775 doi:10.1029/2006GB002914, 2007.

776 Hansen, J., and Nazarenko, L.: Soot climate forcing via snow and ice albedos, *P. Natl.*
777 *Acad. Sci. USA*, 101, 423-428, doi: 10.1073/pnas.2237157100, 2004.

778 Hill, A.F., Rittger, K., Dendup, T., Tshering, D. and Painter, T.H.: How important is
779 meltwater to the Chamkhar Chhu headwaters of the Brahmaputra River?, *Front.*
780 *Earth. Sci.*, 8, 81, doi: 10.3389/feart.2020.00081, 2020.

781 Immerzeel, W.W., van Beek, L.P.H., and Bioerkens, M.F.P.: Climate change will affect
782 the Asian water towers, *Science*, 328, 1382-1385, doi: 10.1126/science.1183188,
783 2010.

784 IPCC: Climate Change 2013: The Physical Science Basis. Contribution of
785 Working Group I to the Fifth Assessment Report of the Intergovernmental Panel
786 on Climate Change. Stocker, T.F., D. Qin, G.-K. Plattner, M. Tignor, S.K. Allen, J.
787 Boschung, A. Nauels, Y. Xia, V. Bex and P.M. Midgley (Ed.). Cambridge
788 University Press, Cambridge, United Kingdom and New York, NY, USA, 1535 pp,
789 doi:10.1017/CBO9781107415324, 2013.

790 Jacobson, M. Z.: Climate response of fossil fuel and biofuel soot, accounting for soot's
791 feedback to snow and sea ice albedo and emissivity, *J. Geophys. Res.*, 109,
792 D21201, doi:10.1029/2004JD004945, 2004.

793 Jenkins, M., Kaspari, S., Kang, S.-C., Grigholm, B., and Mayewski, P.A.: Tibetan
794 Plateau Geladaindong black carbon ice core record (1843-1982): Recent
795 increases due to higher emissions and lower snow accumulation, *Adv. Clim.*
796 *Change Res.*, 7, 132-138, doi: 10.1016/j.accre.2016.07.002, 2016.

797 Kaspari, S., Painter, T.H., Gysel, M., Skiles, S.M., and Schwikowski, M.: Seasonal and
798 elevational variations of black carbon and dust in snow and ice in the Solu-
799 Khumbu, Nepal and estimated radiative forcings, *Atmos. Chem. Phys.*, 14, 8089-
800 8103, doi: 10.5194/acp-14-8089-2014, 2014.

801 Kaspari, S.D., Schwikowski, M., Gysel, M., Flanner, M.G., Kang, S., Hou, S., and
802 Mayewski, P.A.: Recent increase in black carbon concentrations from a Mt.
803 Everest ice core spanning 1860-2000 AD, *Geophys. Res. Lett.*, 38, L04703, doi:
804 10.1029/2010GL046096, 2011.

805 Kopacz, M., Mauzerall, D.L., Wang, J., Leibensperger, E.M., Henze, D.K., and Singh,
806 K.: Origin and radiative forcing of black carbon transported to the Himalayas and
807 Tibetan Plateau, *Atmos. Chem. Phys.*, 11, 2837-2852, doi: 10.5194/acp-11-2837-
808 2011, 2011.

809 Kumar, R., Barth, M.C., Pfister, G.G., Nair, V.S., Ghude, S.D., and Ojha, N.: What
810 controls the seasonal cycle of black carbon aerosols in India?, *J. Geophys. Res.*
811 *Atmos.*, 120, 7788-7812, doi: 10.1002/2015JD023298, 2015.

812 Lack, D.A., Moosmüller, H., McMeeking, G.R., Chakrabarty, R.K., and Baumgardner,
813 D.: Characterizing elemental, equivalent black, and refractory black carbon
814 aerosol particles: a review of techniques, their limitations and uncertainties, *Annl.*
815 *Bioanal. Chem.*, 406, 99-122, doi: 10.1007/s00216-013-7402-3, 2014.

816 Lau, W.K.M., and Kim, K.M.: Fingerprinting the impacts of aerosols on long-term trends
817 of the Indian summer monsoon regional rainfall, *Geophys. Res. Lett.*, 37,
818 L16705, doi: 10.1029/2010GL043255, 2010.

819 Lee, Y.H., Lamarque, J.-F., Flanner, M.G., Jiao, C., Shindell, D.T., Bernsten, T.,
820 Bisiaux, M.M., Cao, J., Collins, W.J., Curran, M., Edwards, R., Faluvegi, G.,
821 Ghan, S., Horowitz, L.W., McConnell, J.R., Ming, J., Myhre, G., Nagashima, T.,
822 Naik, V., Rumbold, S.T., Skeie, R.B., Sudo, K., Takemura, T., Thevenon, F., Xu,
823 B., and Yoon, J.-H.: Evaluation of preindustrial to present-day black carbon and
824 its albedo forcing from Atmospheric Chemistry and Climate Model
825 Intercomparison Project (ACCMIP), *Atmos. Chem. Phys.*, 13, 2607-2634,
826 doi:10.5194/acp-13-2607-2013, 2013.

827 Lelieveld, J., Bourtsoukidis, E., Bruhl, C., Fischer, H., Fuchs, H., Harder, H.,

828 Hofzumahaus, A., Holland, F., Marno, D., Neumaier, M., Pozzer, A., Schlager,
829 H., Williams, J., Zahn, A., and Ziereis, H.: The South Asian monsoon – pollution
830 pump and purifier, *Science*, 361, 270-273, doi: 10.1126/science.aar2501, 2018.

831 Li, S., Yao, T., Tian, L., and Wang, P.: Seasonal transition characteristics of the
832 westerly jet: Study based on field observations at an altitude of 6900 m on the
833 Mt. Xixiabangma Dasuopu glacier, *Chinese Sci. Bull.*, 56, 1912-1920, doi:
834 10.1007/s11434-011-4508-x, 2011.

835 Lindberg, J.D., Douglass, R.E., and Garvey, D.M.: Atmospheric particulate absorption
836 and black carbon measurement, *Appl. Optics*, 38, 2369-2376, doi:
837 10.1364/AO.38.002369, 1999.

838 Liu, X., Xu, B., Yao, T., Wang, N., and Wu, G.: Carbonaceous particles in Muztagh Ata
839 ice core, west Kunlun mountains, China, *Chin. Sci. Bull.*, 53, doi:
840 10.1007/s11434-008-0294-5, 2008.

841 Lund, M.T., Samset, B.H., Skeie, R.B., Watson-Parris, D., Katich, J.M., Schwarz, J.P.,
842 and Weinzierl, B.: Short black carbon lifetime inferred from a global set of aircraft
843 observations, *NPJ Climate and Atmospheric Science*, 1, doi: 10.1038/s41612-
844 018-0040-x, 2018.

845 Marinoni, A., Cristofanelli, P., Laj, P., Duchi, R., Calzolari, F., Decesari, S., Sellegri, K.,
846 Vuillermoz, E., Verza, G.P., Villani, P., and Bonasoni, P.: Aerosol mass and black
847 carbon concentrations, a two year record at NCO-P (5079 m, Southern
848 Himalayas), *Atmos. Chem. Phys.*, 10, 8551-8562, doi: 10.5194/acp-10-8551-
849 2010, 2010.

850 Marinoni, A., Cristofanelli, P., Laj, P., Duchi, R., Putero, D., Calzolari, F., Landi, T.C.,
851 Vuillermoz, E., Maione, M., and Bonasoni, P.: High black carbon and ozone
852 concentrations during pollution transport in the Himalayas: five years of
853 continuous observations at NCO-P global GAW station, *J. Environ. Sci. (China)*,
854 25, 1618-1625, doi: 10.1016/S1001-0742(12)60242-3, 2013.

855 Menking, J.A.: Black carbon measurement of snow and ice using the single particle soot
856 photometer: Method development and an AD 1852-1999 record of atmospheric
857 black carbon from a Mount Logan ice core. M.S. thesis, Central Washington
858 University, Ellensburg, WA, <https://digitalcommons.cwu.edu/etrd/1447>, 2013.

859 Ming, J., Cachier, H., Xiao, C., Qin, D., Kang, S., Hou, S, and Xu, J.: Black carbon
860 record based on a shallow Himalayan ice core and its climatic implications.
861 *Atmos. Chem. Phys.*, 8, 1343–52, doi: 10.5194/acp-8-1343-2008, 2008.

862 Ming, J., Du, Z., Xiao, C., Xu, X., and Zhang, D.: Darkening of the mid-Himalaya
863 glaciers since 2000 and the potential causes, *Environ. Res. Lett.*, 7, 014021, doi:
864 10.1088/1748-9326/7/1/014021, 2012.

865 Mishra, V., Tiwari, A.D., Aadhar, S., Shah, R., Xiao, M., Pai, D.S., and Lettenmaier, D.:
866 Drought and famine in India, 1870-2016, *Geophys. Res. Lett.*, 46, 2075-2083,
867 doi: 10.1029/2018GL081477, 2019.

868 Montanari, L., Basu, B., Spagnoli, A., and Broderick, B.M.: A padding method to reduce
869 edge effects for enhanced damage identification using wavelet analysis, *Mech.*
870 *Syst. Signal Pr.*, 52-52, 264-277, doi: 10.1016/j.ymssp.2014.06.014, 2015.

871 Mooley, D.A., Parthasarathy, B., Sontakke, N.A., Munot, A.A.: Annual rain-water over
872 India, its variability and impact on the economy, *J. Climatol.*, 1, 167-186, doi:
873 10.1002/joc.3370010206, 1981.

874 Nair, V.S., Babu, S.S., Moorthy, K.K., Sharma, A.K., Marinoni, A., and Ayai: Black
875 carbon aerosols over the Himalayas: direct and surface albedo forcing, *Tellus*
876 *Ser. B Chem. Phys. Meteorol.*, 65, 1-14, doi: 10.3402/tellusb.v65i0.19738, 2013.

877 Negi, P.S., Pandey, C.P., and Singh, N.: Black carbon aerosol in the ambient air of
878 Gangotri Glacier valley of north-western Himalaya in India, *Atmos. Environ.*, 214,
879 116879, doi: 10.1016/j.atmosenv.2019.116879, 2019.

880 Niu, H., Kang, S., Shi, X., Paudyal, R., He, Y., Li, G., Wang, S., Pu, T., and Shi, X.: In-
881 situ measurements of light-absorbing impurities in snow of glacier on Mt. Yulong
882 and implications for radiative forcing estimates, *Sci. Total Environ.*, 581-582, 848-
883 856, doi: 10.1016/j.scitotenv.2017.01.032, 2017.

884 Novakov, T., Ramanathan, V., Hansen, J.E., Kirchstetter, T.W., Sato, M., Sinton, J.E.,
885 and Sathaye, J.A., Large historical changes of fossil-fuel black carbon aerosols,
886 *Geophys. Res. Lett.*, 30, 1324, doi: 10.1029/2002GL016345, 2003.

887 Ogren, J.A., and Charlson, R.J.: Elemental carbon in the atmosphere: cycle and
888 lifetime, *Tellus*, 35B, 241-254, doi: 10.1111/j.1600-0889.1983.tb00027.x, 1983.

889 Parthasarathy, B., Sontakke, N.A., Monot, A.A., and Kothawale, D.R.: Droughts/floods
890 in the summer monsoon season over different meteorological subdivisions of
891 India for the period 1871-1984, *Int. J. Climatol.*, 7, 57-70, doi:
892 10.1002/joc.3370070106, 1987.

893 Petzold, A., Ogren, J.A., Fiebig, M., Laj, P., Li, S.-M., Baltensperger, U., Holzer-Popp,
894 T., Kinne, S., Pappalardo, G., Sugimoto, N., Wehrli, C., Wiedensohler, A., and
895 Zhang, X.-Y.: Recommendations for reporting “black carbon” measurements,
896 *Atmos. Chem. Phys.*, 13, 8365-8379, doi: 10.5194/acp-13-8365-2013, 2013.

897 Rahaman, W., Chatterjee, S., Ejaz, T., and Thamban, M.: Increased influence of ENSO
898 on Antarctic temperature since the Industrial Era, *Sci. Rep-UK.*, 9, 6006, doi:
899 10.1038/s41598-019-42499-x, 2019.

900 Ramanathan, V. and Carmichael, G.: Global and regional climate changes due to black
901 carbon, *Nature Geosci.*, 1, 221–227, doi:10.1038/ngeo156, 2008.

902 Ramanathan, V., Ramana, M.V., Roberts, G., Kim, D., Corrigan, C., Chung, C., and
903 Winker, D.: Warming trends in Asia amplified by brown cloud solar absorption,
904 *Nature*, 448, 575-578, doi: 10.1038/nature06019, 2007.

905 Raper, S.C.B., and Braithwaite, R.J.: Low sea level rise projections from mountain
906 glaciers and icecaps under global warming, *Nature*, 439, 311-313, doi:
907 10.1038/nature04448, 2006.

908 Reddy, M.S., and Boucher, O.: A study of the global cycle of carbonaceous aerosols in
909 the LMDZT general circulation model, *J. Geophys. Res.*, 109, D14202, doi:
910 10.1029/2003JD0040-48, 2004.

911 Reddy, M.S., and Boucher, O.: Climate impact of black carbon emitted from energy
912 consumption in the world’s regions, *Geophys. Res. Lett.*, 34, L11802, doi:
913 10.1029/2006GL028904, 2007.

914 Ross, A.B., Jones, J.M., Chaiklangmuang, S., Pourkashanian, M., Williams, A., Kubica,
915 K., Andersson, J.T., Kerst, M., Danihelka, P., and Bartle, K.D.: Measurement and
916 prediction of the emission of pollutants from the combustion of coa and biomass
917 in a fixed bed furnace, *Fuel*, 81, 571-582, doi:10.1016/S0016-2361(01)00157-0,
918 2002.

919 Samset, B.H., Myhre, G., Herber, A., Kondo, Y., Li, S.-M., Moteki, N., Koike, M.,

920 Oshima, N., Schwarz, J.P., Balkanski, Y., Bauer, S.E., Bellouin, N., Bernsten,
921 T.K., Bian, H., Chin, M., Diehl, T., Easter, R.C., Ghan, S.J., Iversen, T., Kirkevag,
922 A., Lamarque, J.-F., Lin, G., Liu, X., Penner, J.E., Schulz, M., Seland, O., Skeie,
923 R.B., Stier, P., Takemura, T., Tsigardis, K., and Zhang, K.: Modelled black
924 carbon radiative forcing and atmospheric lifetime in AeroCom Phase II
925 constrained by aircraft observations, *Atmos. Chem., Phys.*, 14, 12465-12477,
926 doi: 10.5194/acp-14-12465-2014, 2014.

927 Samsonov, Y.N., Ivanov, V.A., McRae, D.J., and Baker, S.P.: Chemical and dispersal
928 characteristics of particulate emissions from forest fires in Siberia, *Int. J. Wildland
929 Fire*, 21, 818-827, doi: 10.1071/WF11038, 2012.

930 Schwarz, J.P., Gao, R.S., Fahey, D.W., Thomson, D.S., Watts, L.A., Wilson, J.C.,
931 Reeves, J.M., Darbeheshti, M., Baumgardner, D.G., Kok, G.L., Chung, S.H.,
932 Schulz, M., Hendricks, J., Lauer, A., Karcher, B., Slowik, J.G., Rosenlof, K.H.,
933 Thompson, T.L., Langford, A.O., Loewenstein, M., and Aikin, K.C.: Single-particle
934 measurements of midlatitude black carbon and light-scattering aerosols from the
935 boundary layer to the lower stratosphere, *J. Geophys. Res. Atmos.*, 111,
936 D16207, doi: 10.1029/2006JD007076, 2006.

937 Scott, C.A., Zhang, F., Mukherji, A., Immerzeel, W., Mustafa, D., and Bharati, L.: Water
938 in the Hindu Kush Himalaya. In: Wester, P., Mishra, A., and Shrestha, A. (eds):
939 The Hindu Kush Himalaya Assessment. Springer, Cham, doi: 10/1007/978-3-
940 319-92288-1_8, 2019.

941 Solanki, R., and Singh, N.: LiDAR observations of the vertical distribution of aerosols in
942 free troposphere: Comparison with CALIPSO level-2 data over central
943 Himalayas, *Atmos. Env.*, 99, 227-238, doi: 10.1016/j.atmosenv.2014.09.083,
944 2014.

945 Stothers, R.B.: The great Tambora eruption in 1815 and its aftermath, *Science*, 224,
946 1191-1198, doi: 10.1126/science.224.4654.1191, 1984.

947 Su, H., Liu, Q., and Li, J.: Alleviating border effects in wavelet transforms for nonlinear
948 time-varying signal analysis, *Adv. Electr. Comput. En.*, 11, 55-60, doi:
949 10.4316/AECE.2011.03009, 2011.

950 Thapa, U.K., St. George, S., Kharal, D.K., and Gaire, N.P.: Tree growth across the
951 Nepal Himalaya during the last four centuries, *Prog. Phys. Geog.*, 41, 478-495,
952 doi: 10.1177/0309133317714247, 2017.

953 Thind, P.S., Chandel, K.K., Sharma, S.K., Mandal, T.K., and John, S.: Light-absorbing
954 impurities in snow of the Indian Western Himalayas: impact on snow albedo,
955 radiative forcing, and enhanced melting, *Environ. Sci. Pollut. R.*, 26, 7566-7578,
956 doi: 10.1007/S11356-019-04183-5, 2019.

957 Thompson, L.G., Yao, T., Mosley-Thompson, E., Davis, M.E., Henderson, K.A., and Lin,
958 P.-N.: A high-resolution millennial record of the south Asian monsoon from
959 Himalayan ice cores, *Science*, 289, 1916-1919, doi:
960 10.1126/science.289.5486.1916, 2000.

961 Torrence, C., and Compo, G.P.: A practical guide to wavelet analysis, *B. Am. Meteorol.
962 Soc.*, 79, 61-78, doi: 10.1175/1520-0477(1998)079<0061:APGTWA>2.0.CO;2,
963 1998.

964 Tosca, M.G., Randerson, J.T., Zender, C.S., Flanner, M.G., and Rasch, P.J.: Do

965 biomass burning aerosols intensify drought in equatorial Asia during El Niño?,
966 *Atmos. Chem. Phys.*, 10, 3515-3528, doi: 10.5194/acpd-9-23319-2009, 2010.

967 Uglietti, C., Gabrielli, P., Olesik, J.W., Lutton, A., and Thompson, L.G.: Laerge variability
968 of trace element mass fractions determined by ICP-SFMS in ice core samples
969 from worldwide high altitude glaciers, *Appl. Geochem.*, 47, 109-121, doi:
970 10.1016/j.apgeochem.2014.05.019, 2014.

971 Wang, M., Xu, B., Kaspari, S.D., Gleixner, G., Schwab, V.F., Zhao, H., Wang, H., and
972 Yao, P.: Century-long record of black carbon in an ice core from the Eastern
973 Pamirs: Estimated contributions from biomass burning, *Atmos. Env.*, 115, 79-88,
974 doi: 10.1016/j.atmosenv.2015.05.034, 2015.

975 Wendl, I.A., Menking, J.A., Färber, R., Gysel, M., Kaspari, S.D., Laborde, M.J.G., and
976 Schwikowski, M.: Optimized method for black carbon analysis in ice and snow
977 using the Single Particle Soot Photometer, *Atmos. Meas. Tech.*, 7, 2667-2681,
978 doi: 10.5194/amt-7-2667-2014, 2014.

979 Xu, B., Cao, J., Hansen, J., Yao, T., Joswia, D.R., Wang, N., Wu, G., Wang, M., Zhao,
980 H., Yang, W., Liu, X., and He, J.: Black soot and the survival of Tibetan glaciers,
981 *P. Natl. Acad. Sci. USA*, 106, 22114-22118, doi: 10.1073/pnas.0910444106,
982 2009.

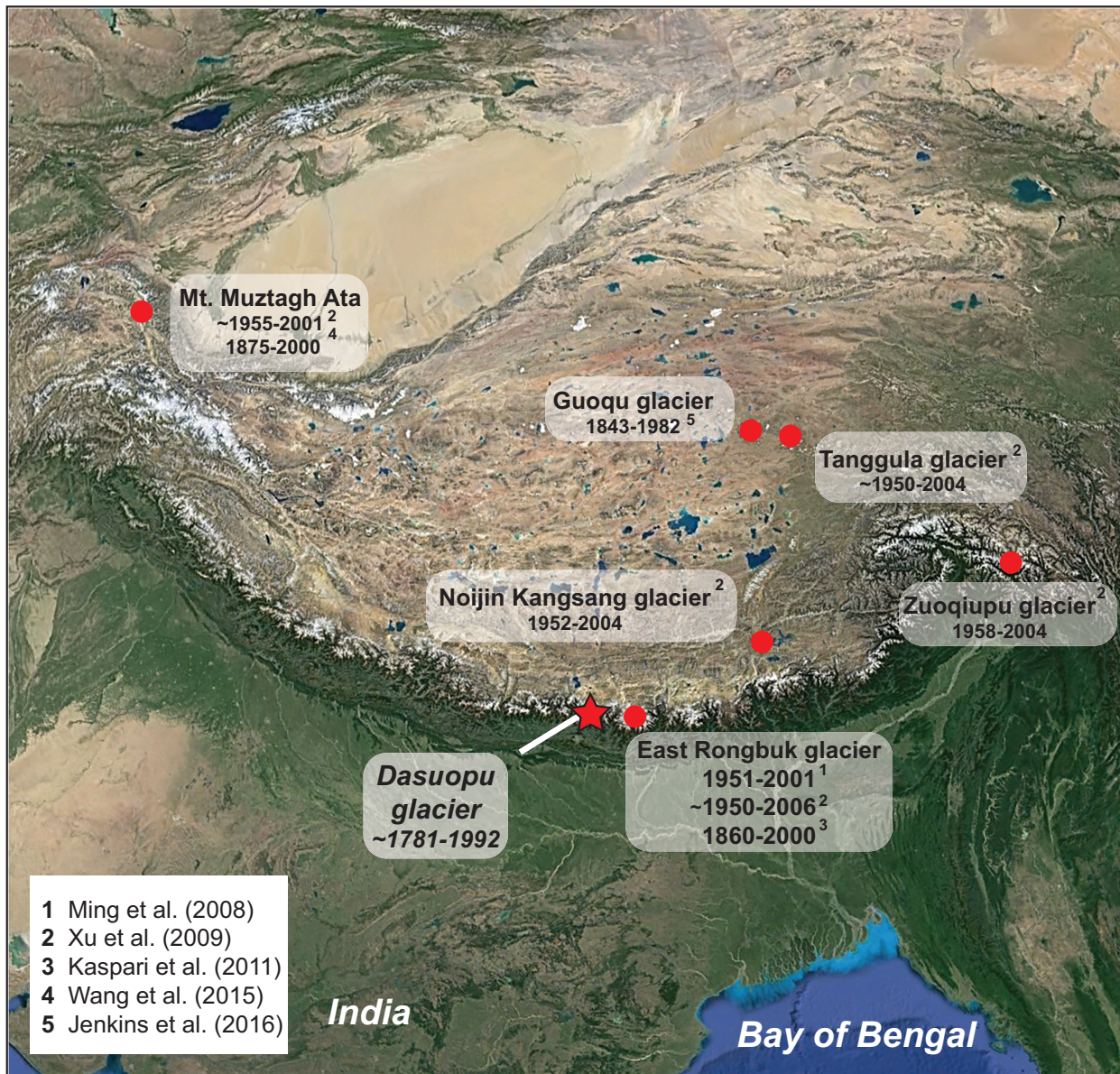
983 Xu, B., Cao, J., Joswiak, D.R., Liu, X., Zhao, H., and He, J.: Post-depositional
984 enrichment of black soot in snow-pack and accelerated melting of Tibetan
985 glaciers, *Environ. Res. Lett.*, 7, 014022, doi: 10.1088/1748-9326/7/1/014022,
986 2012.

987 Yang, M., Yao, T., Wang, H., and Gou, X.: Climatic oscillations over the past 120 kyr
988 recorded in the Guliya ice core, China, *Quartern. Int.*, 154-155, 11-18, doi:
989 10.1016/j.quaint.2006.02.015, 2006.

990 Zhang, Y., Kang, S., Sprenger, M., Cong, Z., Gao, T., Li, C., Tao, S., Li, X., Zhong, X.,
991 Xu, M., Meng, W., Neupane, B., Qin, X., and Sillanpaa, M.: Black carbon and
992 mineral dust in snow cover on the Tibetan Plateau, *The Cryosphere*, 12, 413-
993 431, doi: 10.5194/tc-12-413-2018, 2018.

994

995 Figure 1:



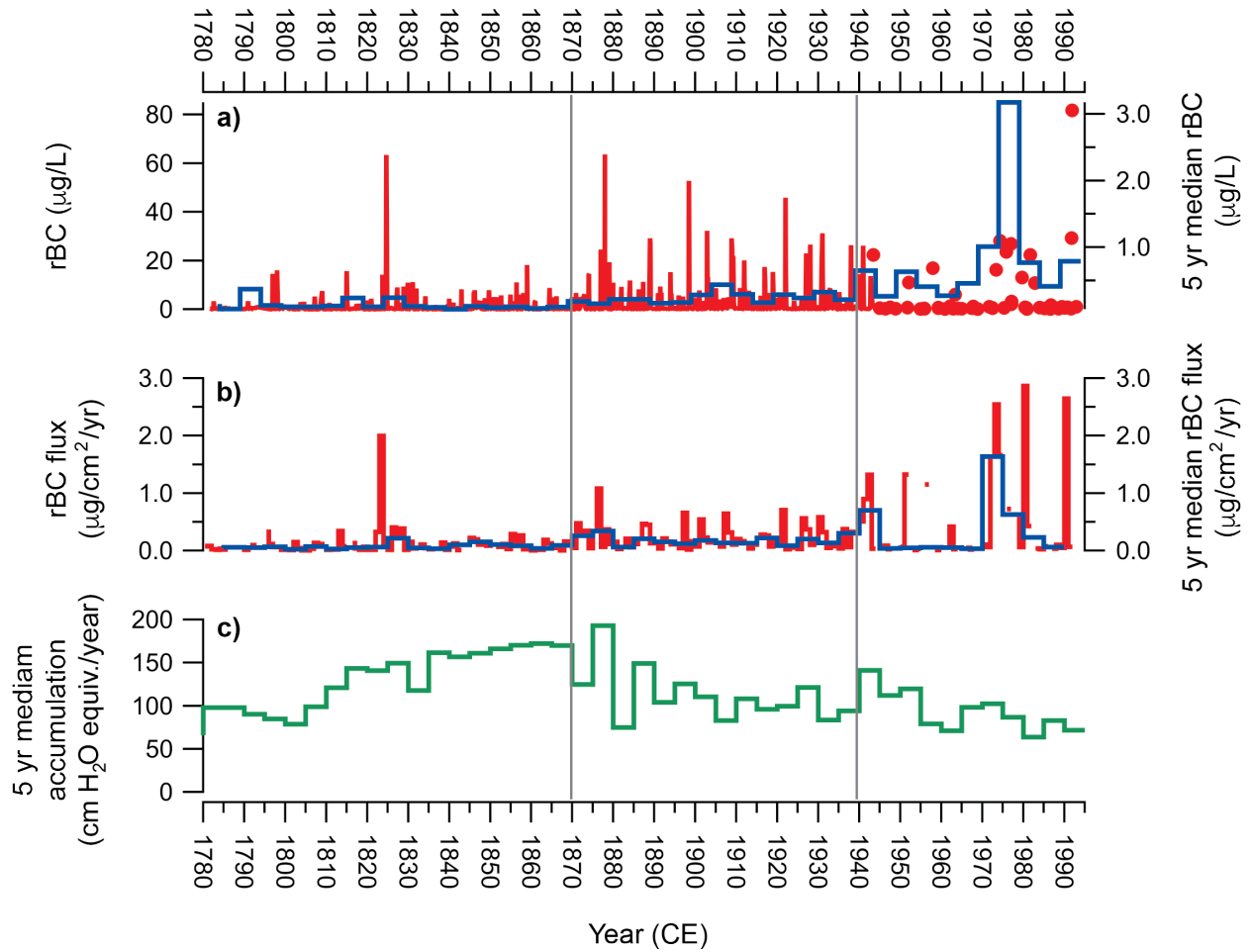
996

Source: "Tibetan Plateau" 28.38°N, 85.72°E. © Google Earth, Image: Landsat / Copernicus. 11/30/2016. 11/20/2019.

997 Fig. 1: The location of Dasuopu glacier, Mt. Xixiabangma and the location of other ice
998 cores that have provided a historical record of BC deposition in the region. The span of
999 each BC record is indicated.

1000

1001 Figure 2:

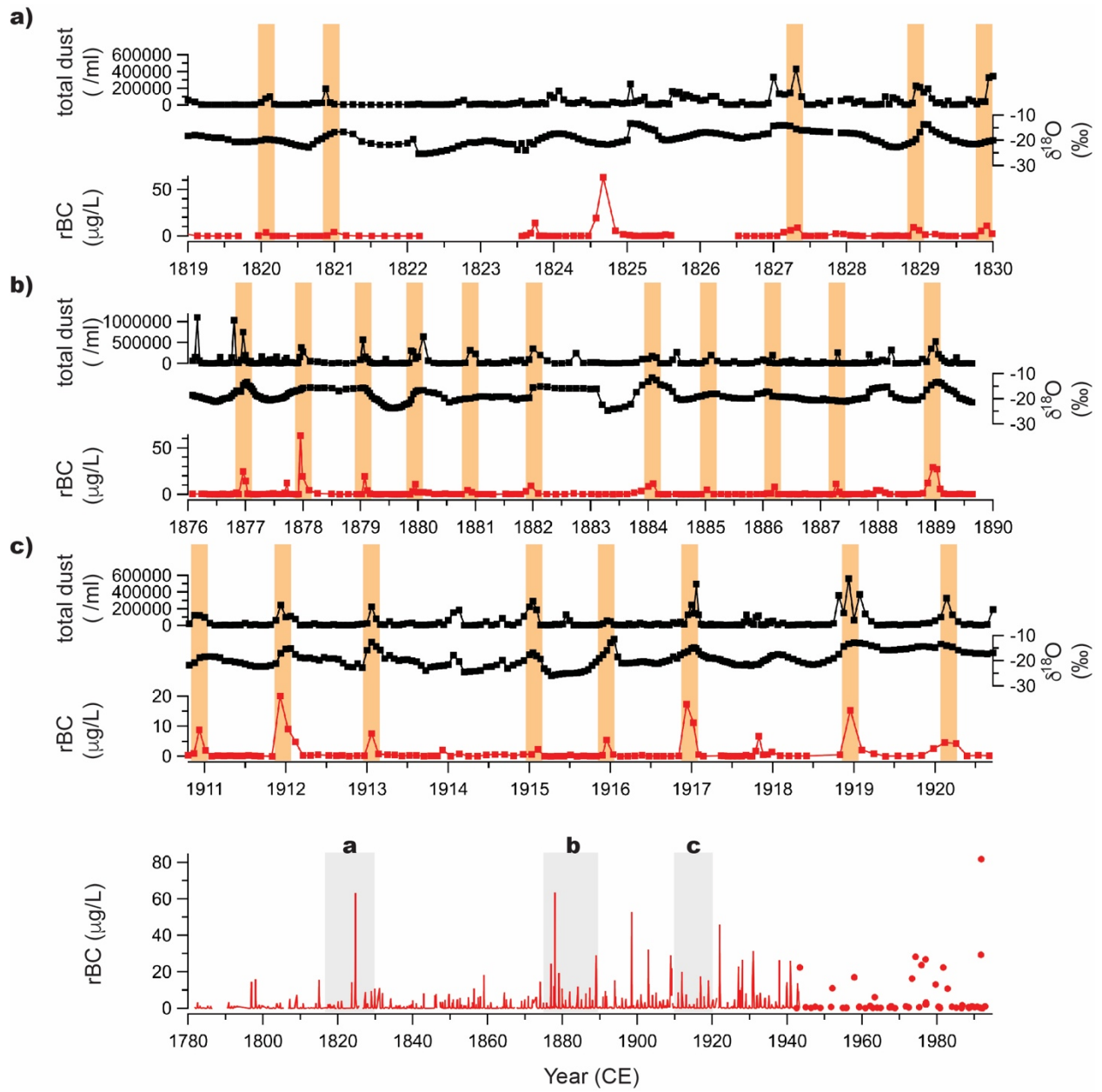


1002

1003 Fig. 2: a) the rBC record from the Dasuopu ice core (red). Red dots indicate discrete firm
1004 samples. The 5 year median is indicated (blue); b) the rBC deposition flux onto
1005 Dasuopu glacier (red) with the 5 year median (blue); c) the annual snow accumulation
1006 record for the Dasuopu ice core (Davis et al., 2005).

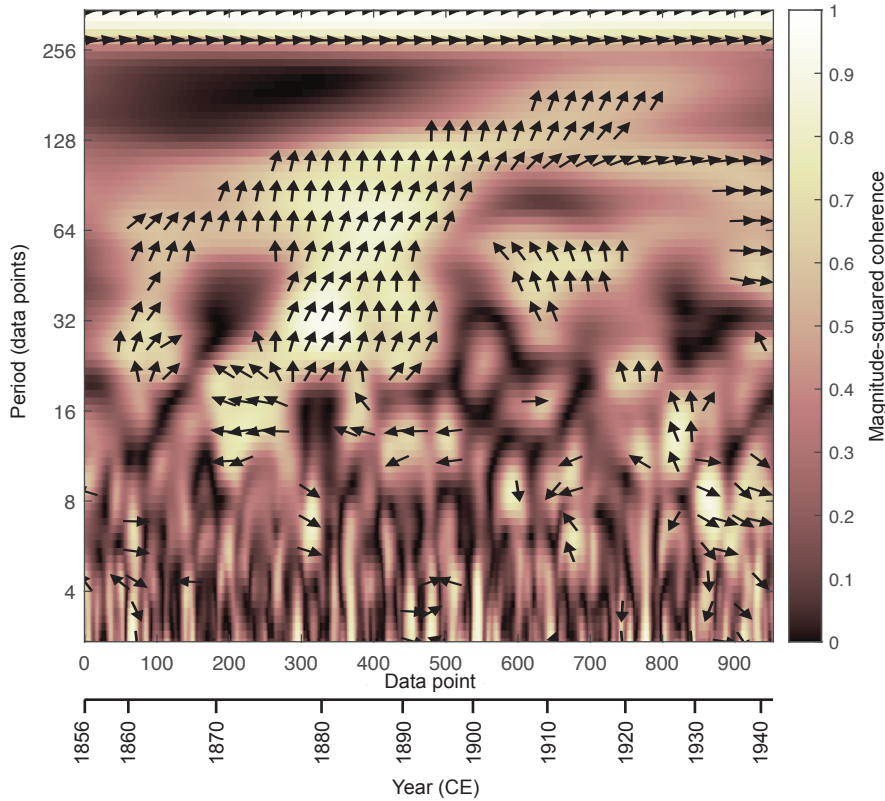
1007

1008 Figure 3:



1009
1010

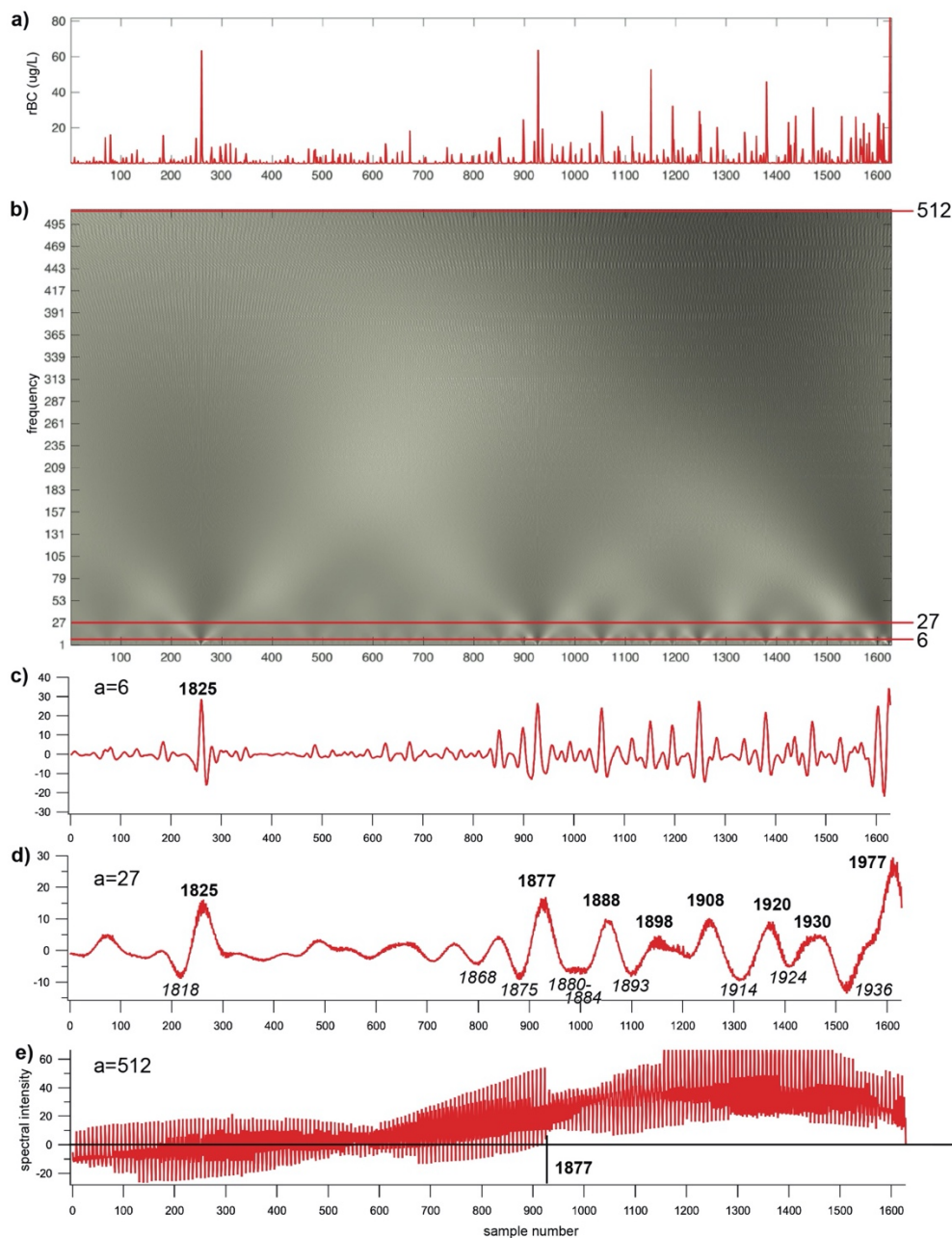
d)



1011
 1012
 1013
 1014
 1015
 1016
 1017
 1018
 1019
 1020
 1021
 1022
 1023

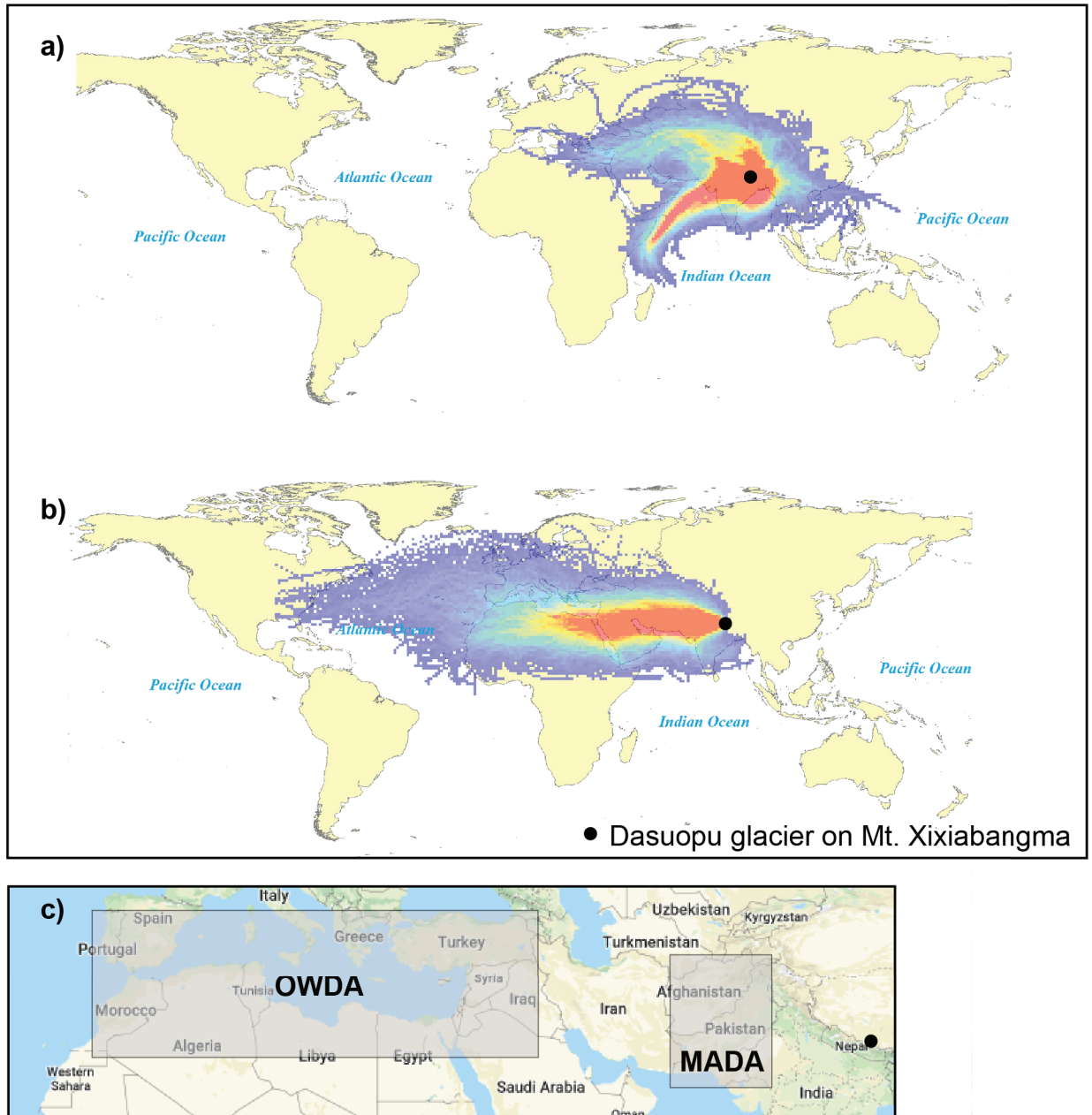
Fig. 3: Peaks in the rBC record compared to the total dust and $\delta^{18}\text{O}$ records (Thompson et al., 2000) over 3 time intervals (a: 1819 - 1830, b: 1876 - 1890, c: 1911 - 1921 CE) in the Dasuopu ice core. Note that peaks in the rBC record are associated with depleted $\delta^{18}\text{O}$ and increased dust deposition. The spectral coherence between rBC and $\delta^{18}\text{O}$ between 1856 – 1943 CE (d) shows strong magnitude-squared coherence at a long period (~ 21 year) with no phase lag (as shown by arrows oriented in radian space (ie: arrow oriented to right indicates no phase lag; arrows oriented to the left indicate anti-phase relationship), strong magnitude-squared coherence between 2 and 10 years with a 0.5 – 2.5 year phase lag between 1878 – 1900 CE, and strong magnitude-squared coherence with no phase lag between 1910 – 1943 CE.

1024 Figure 4:



1025

1026 Fig. 4: The spectral analysis of the Dasuopu rBC concentration record. Sample number
1027 1 is located at the bottom of the ice core (1781 CE) and sample number 1628 is at the
1028 top of the firn section (1992 CE). a) is the rBC record plotted relative to sample number;
1029 b) is the spectral analysis showing variance across all frequency scales relative to
1030 sample number ranging from a = 2 to a = 512. Darker shades indicate relatively
1031 stronger (more positive) coherence between the wavelet and the rBC record, as
1032 indicated in the spectral coefficients; c, d, e) are the spectral coefficients relative to
1033 sample number for frequency scales a = 6, 27, and 512 respectively.
1034



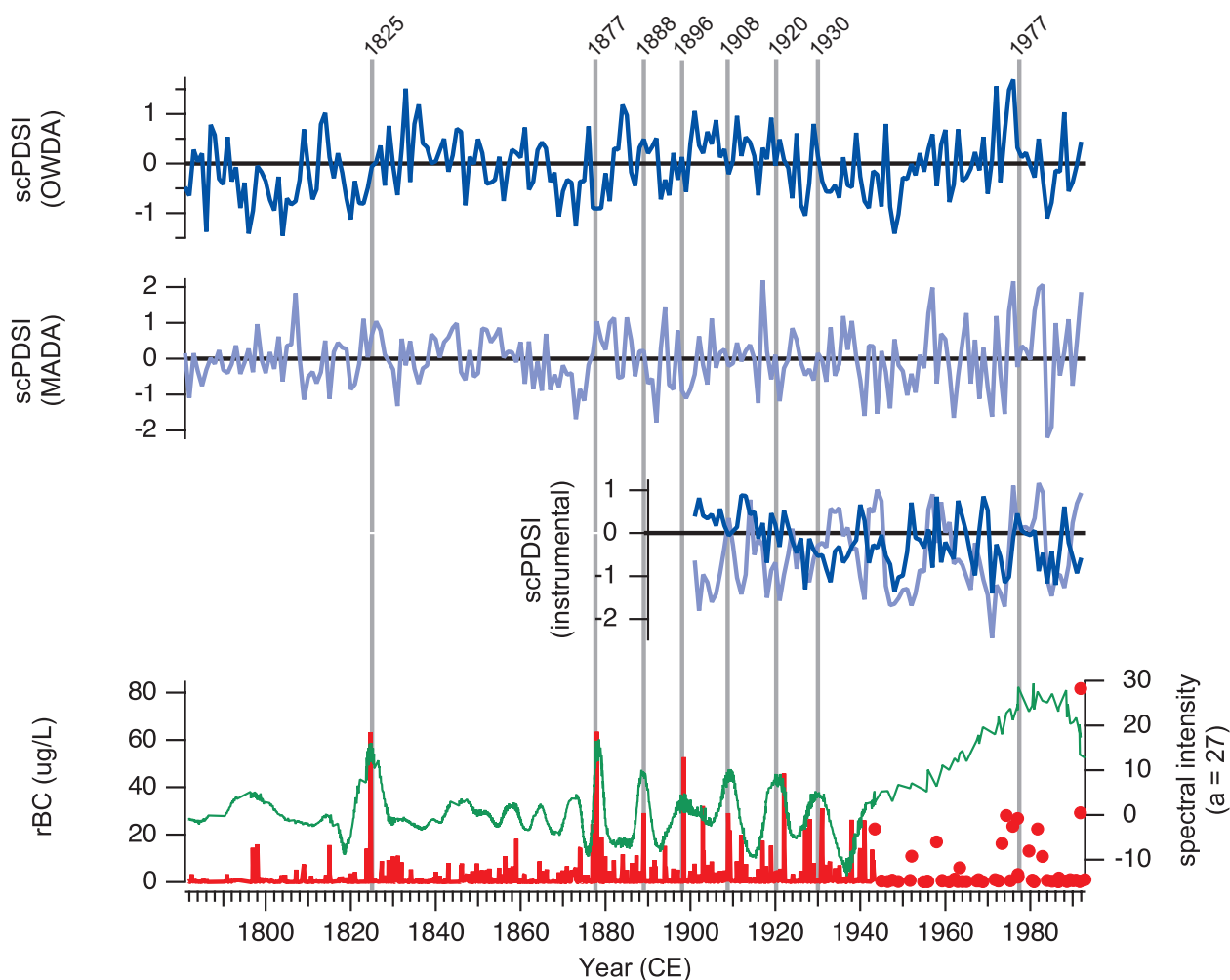
Source: © 2020 Google

1036

1037 Fig. 5: Frequency of back trajectories for airmasses arriving at the Mt. Xixiabangma a)
 1038 July, b) January. Red and blue indicate a higher frequency and lower frequency air
 1039 mass flow paths, respectively. The area included in the Old World Drought Atlas
 1040 (OWDA; Cook et al., 2015) and the Monsoon Asia Drought Atlas (MADA; Cook et al.,
 1041 2010) reconstructions is indicated (c).

1042

1043 Figure 6:

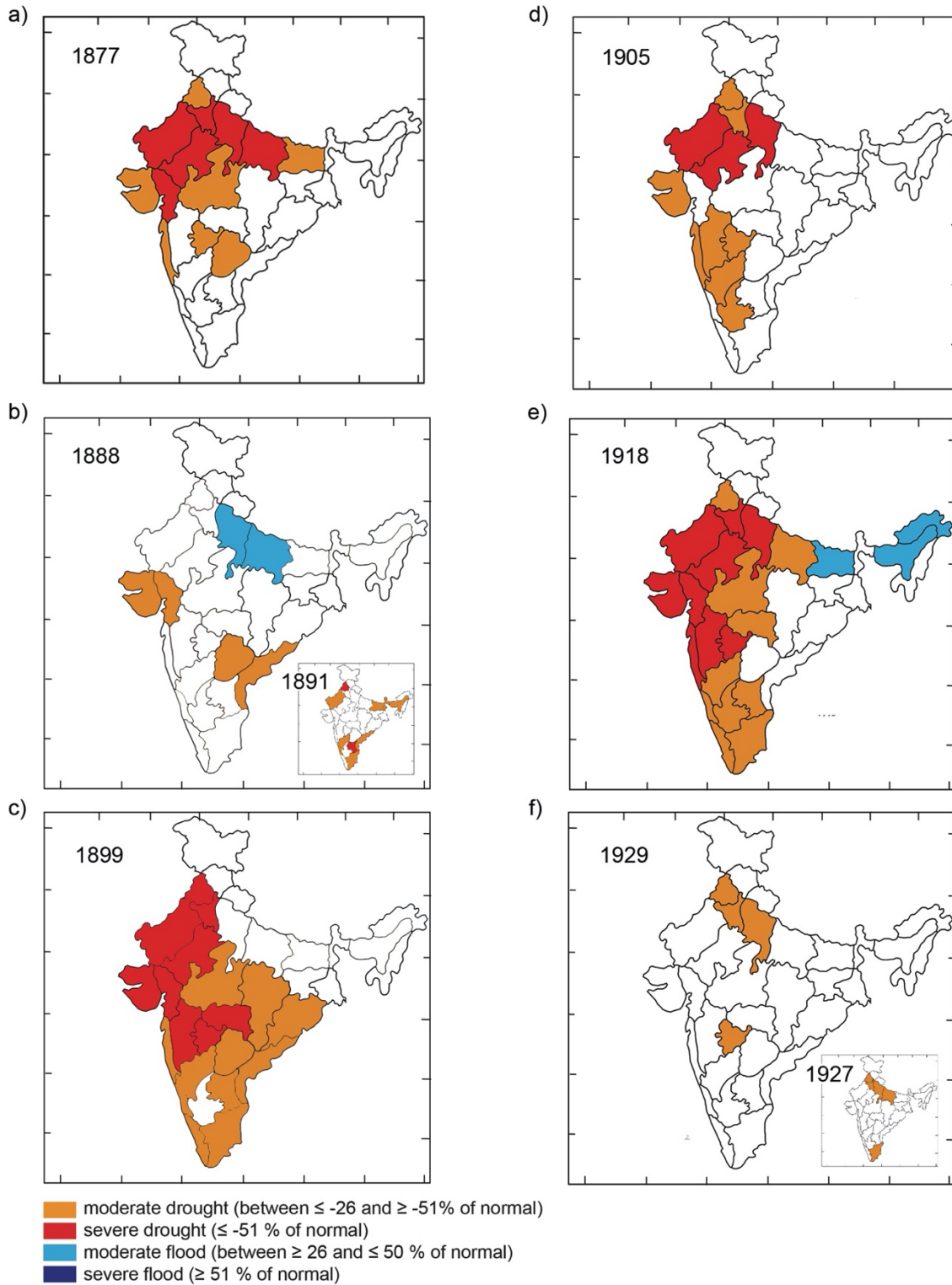


1044

1045 Fig. 6: The Dasuopu rBC record (in red) compared to regional reconstructed and
1046 instrumental climate records from the Old World Drought Atlas (OWDA; dark blue) and
1047 the Monsoon Asia Drought Atlas (MADA; light blue). Note the correspondence between
1048 negative self-calibrating Palmer Drought Severity Index (scPDSI) and periods of high
1049 rBC deposition. Data for both the reconstructed and instrumental climate records are
1050 obtained from; OWDA (drought.memphis.edu/OWDA/) and MADA
1051 (drought.memphis.edu/MADA).

1052

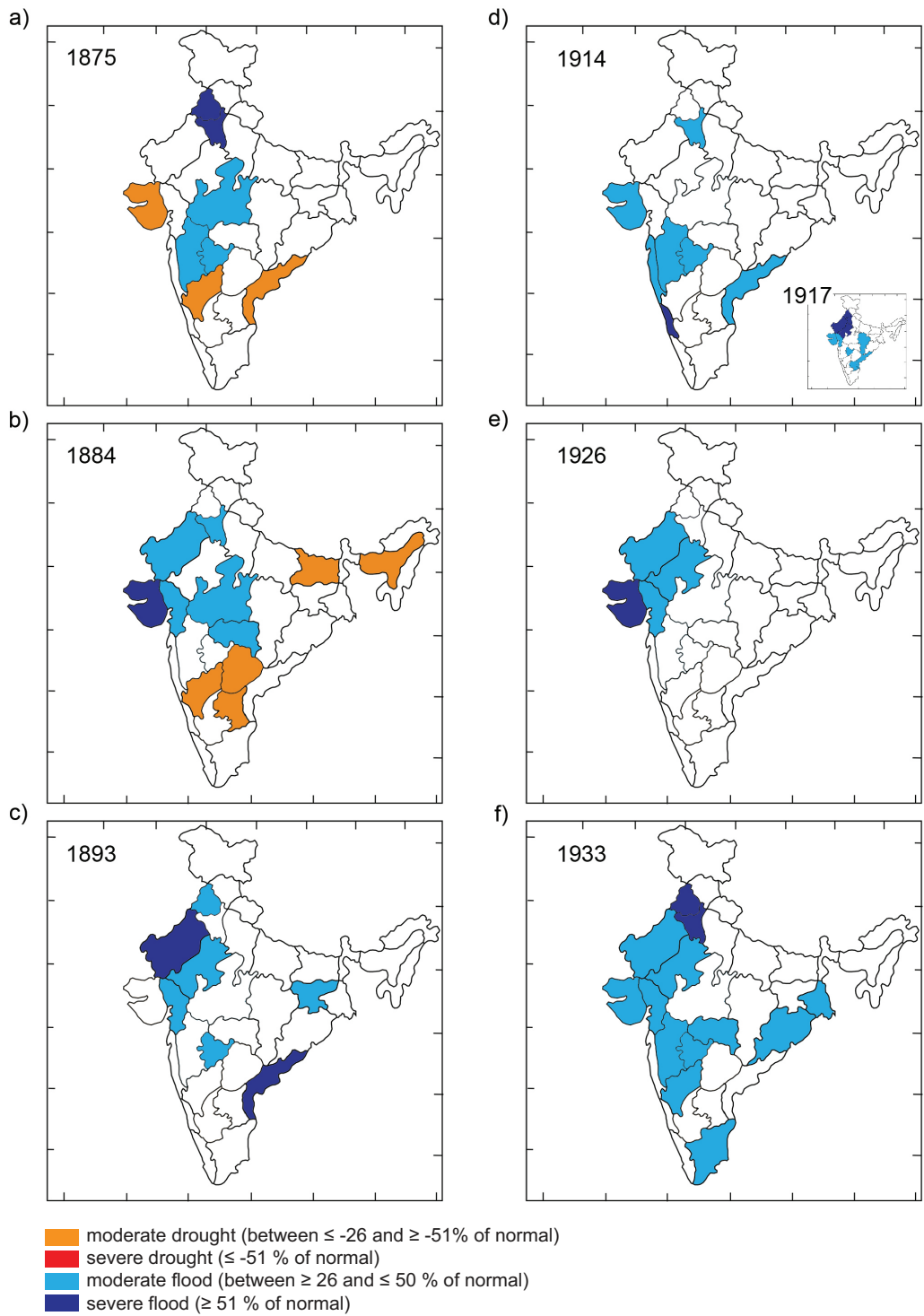
1053 Figure 7:



1054

1055 Fig. 7: The distribution of meteorologic subdivisions in NW India reporting drought
1056 during periods of high spectral intensity at a = 27 scale.
1057

1058 Figure 8:



1059
1060
1061
1062
1063

Fig. 8: The distribution of meteorologic subdivisions in NW India reporting flood conditions during periods of low spectral intensity at a = 27 scale.

1064 Table 1:

trace element (ⁿ)	total <i>r_s</i>	pre-1877 <i>r_s</i>	post-1877 <i>r_s</i>	EF total <i>r_s</i>	EF pre-1877 <i>r_s</i>	EF post-1877 <i>r_s</i>
Al ⁽⁹¹⁵⁾	0.22	0.40	<i>-0.08</i>	-0.45	-0.40	-0.55
As ⁽⁹¹⁴⁾	0.23	0.41	<i>-0.06</i>	-0.41	-0.41	-0.44
Ba ⁽⁹¹⁶⁾	0.26	0.43	<i>-0.07</i>	-0.24	-0.25	-0.28
Bi ⁽⁸⁵⁷⁾	0.20	0.40	<i>-0.10</i>	-0.37	-0.33	-0.44
Cd ⁽⁹¹⁶⁾	0.23	0.37	<i>-0.07</i>	-0.5	-0.48	-0.62
Co ⁽⁹¹⁵⁾	0.23	0.41	<i>-0.09</i>	-0.38	-0.40	-0.42
Cr ⁽⁹¹⁵⁾	0.19	0.38	<i>-0.09</i>	-0.56	-0.53	-0.64
Cs ⁽⁹¹³⁾	0.25	0.41	<i>-0.04</i>	-0.39	-0.35	-0.48
Fe ⁽⁹¹⁵⁾	0.23	0.42	<i>-0.07</i>			
Ga ⁽⁹¹⁵⁾	0.22	0.39	<i>-0.07</i>	-0.57	-0.54	-0.68
Mg ⁽⁹¹⁵⁾	0.24	0.44	<i>-0.09</i>	-0.21	-0.20	-0.22
Mn ⁽⁹¹⁵⁾	0.24	0.44	<i>-0.10</i>	<i>0.02</i>	<i>-0.01</i>	<i>0.06</i>
Mo ⁽⁹¹⁵⁾	0.22	0.37	<i>-0.08</i>	-0.54	-0.52	-0.63
Nb ⁽⁹¹⁵⁾	0.21	0.36	<i>-0.04</i>	-0.48	-0.46	-0.59
Ni ⁽⁹¹⁵⁾	0.22	0.39	<i>-0.09</i>	-0.5	-0.50	-0.57
Pb ⁽⁹¹⁶⁾	0.23	0.40	<i>-0.08</i>	-0.31	-0.31	-0.35
Rb ⁽⁹¹⁴⁾	0.27	0.43	<i>-0.05</i>	-0.49	-0.47	-0.60
Sb ⁽⁹¹⁶⁾	0.19	0.38	<i>-0.07</i>	-0.56	-0.52	-0.65
Ti ⁽⁹¹⁴⁾	0.23	0.41	<i>-0.08</i>	-0.28	-0.25	-0.42
Tl ⁽⁹¹⁶⁾	0.24	0.42	<i>-0.08</i>	-0.52	-0.49	-0.62
U ⁽⁹¹⁶⁾	0.24	0.41	<i>-0.07</i>	-0.29	-0.29	-0.34
V ⁽⁹¹⁵⁾	0.24	0.40	<i>-0.07</i>	-0.52	-0.51	-0.63
Zn ⁽⁹¹⁵⁾	0.15	0.26	<i>-0.06</i>	-0.53	-0.52	-0.63

1065

1066 Table 1. The Spearman correlation coefficient (r_s , $\alpha=0.01$) for trace elements and the
 1067 trace element enrichment factor (EF) relative to rBC concentration throughout the
 1068 Dasuopu ice core. Italics indicate a non-statistically significant r_s .